PCCP

Accepted Manuscript

ROYAL SOCIETY OF CHEMISTRY

www.rsc.org/pccp

Time Dependent DFT Investigation of the Optical Properties of Artificial Light Harvesting Special Pairs

Neha Agnihotri[1*] and Ronald P. Steer[2*]

[1]Department of Physics, Indian Institute of Technology (BHU), Varanasi-221005, India

[2]Department of Chemistry, University of Saskatchewan, Saskatoon, SK, Canada, S7N 5C9

* to whom correspondence should be addressed

email: ron.steer@usask.ca n.agnihotri6@gmail.com

phone: 1-306-966-4667(RPS) 91-893-387-3665(NA)

Keywords: light harvesting, cofacial bis-porphyrins, special pair, DFT, TDDFT

Abstract:

Computational modeling of selected artificial special pairs has been carried out. The structures chosen are bio-inspired molecular models of the light harvesting system II that have been previously investigated experimentally. Time-dependent density functional theory calculations have been employed to characterize the inter-macrocycle interactions resulting from two zinc porphyrins that are covalently linked with rigid linkers that vary the inter-porphyrin distance and the inter-planar angle in a C_{2v} framework. The effects of varying the linker structure have been explored for electronic states with energies up to and including the Soret-correlated states in the dimer. An expansion of the Gouterman four orbital model for the monomers to an eight orbital model in the dimers provides a reasonable explanation of the inter-macrocycle interactions and provides insight into their experimental properties.

1. Introduction:

Photosynthetic organisms are some of Nature's most efficient creations and therefore hold great promise as models for the design of artificial systems for harvesting sunlight. A typical light harvesting system (*e.g.* LH II found in purple bacteria[1-7]) contains a series of antenna molecules involving bacteriochlorophylls, carotenoids and electron transport accessories linked to central special pairs. In LH II, antenna bacteriochlorophylls absorb the incident light and transfer the energy to the reaction centers, promoting them to an electronically excited state. Initial charge separation occurs when an electron is rapidly transferred from this excited state to the primary electron acceptor inside the reaction centre.[8-11] Excitonic interactions inside the central special pair may also contribute to the charge separation process.[12] It follows naturally that a rich literature describing artificial systems that mimic these light harvesting systems has developed, with the central special pair receiving particular attention.[13-17] However, realizing an efficient working mimic has proved to be extraordinarily difficult due to the inter-dependence of the relevant structure-property relationships on many factors.[18,19]

Typical special pairs are slipped cofacial dimers of chlorophylls (in plants) or bacteriochlorophylls (in purple bacteria) that exist in various relative arrangements depending on the nature of the photosystem and the organism. Their photophysical properties are highly dependent on the extent of their variable interplanar π-π interaction, a parameter that needs to be controlled in artificial systems. The photophysical properties of many dimers, trimers and larger oligomers held together by covalent and coordinate bonds have been determined.[14] The photoactive chromophores of the special pair can be arranged either side-by-side (J-aggregates) or face-to-face (H-aggregates) inside the LH II system. Here we focus on structures in which two chromophores are placed together in the face-to-face configuration in the central special pair, and are bridged with a linker at a particular distance and orientation in order to obtain the desired geometry. Harvey and co-workers[20] have shown that rigid linkers are more efficient than flexible ones, as a desired structure is more easily attained with limited degrees of freedom. The most popular ones are shown in Fig. 1.

Porphyrins have macrocyclic skeletons and photophysical properties similar to those of chlorophyll and are often the preferred components for the synthesis of artificial special pairs. Porphyrins held together with rigid linkers thus mimic naturally occurring systems and have

found applications in synthetic light harvesting systems, in opto-electronic devices and as dyes in dye-sensitized solar cells. It is, therefore, of interest to determine the bridging unit that allows the most efficient electronic communication between two porphyrin macrocycles.

Chang, Nocera and co-workers[21-27] were the first to propose and investigate experimentally the properties of synthetic cofacial ("PACMAN") bis-porphyrins held in a face-to-face arrangement with different rigid linkers. Harvey, Guilard and co-workers[28-41] have proposed additional models for synthetic special pairs and have explored their photophysical properties experimentally, supplemented by theoretical calculations in some cases.

Our objective is to investigate the electronic properties of the artificial special pairs that are the bioinspired molecular models of LH II found in purple bacteria using density functional theory (DFT) and time-dependent DFT(TDDFT) computations. This approach has proved successful with an axially-linked metalloporphyrin dimer[42] in which an extension of Gouterman's four-orbital model[43,44] proved to be useful in interpreting its properties. Here, we report similar computations on a series of ten artificial special pairs containing metalloporphyrin chromophores linked peripherally by rigid linkers that orient the macrocycles at different interplanar angles and spacings. The parameters considered in designing these systems are described below and are given as footnotes to Table 2.

2. Computational Approaches:

The ground state geometries of the five unsubstituted zinc porphyrin dimers $(ZnP)_2X$, along with five zinc triphenyl porphyrin dimers, $(ZnTriPP)_2X$, covalently linked with five different rigid linkers, X = DPA, DPB, DPO, DPS and DPX (the respective hetero atoms in DPO, DPS and DPX are O, S and O), were fully optimized employing analytical gradient techniques *in vacuo*. The linkers are all rigid aromatic structures containing two benzene rings fused in ways designed to vary the distance between the carbon atoms in their *ortho*-positions and the angles at which the macrocycle planes of the linked porphyrins will lie. The local minimum energy structures were found by determining that all of the harmonic frequencies were real. Initially, DFT with Becke's three parameter (B3) exchange functional together with the Lee–Yang–Parr (LYP) non-local correlation functional with an optimized weight of the exact HF exchange (B3LYP) was employed[45-47] in conjunction with a standard 6-31G(d) basis set. Recent results have revealed that the 6-31G(d) basis set can adequately predict the molecular geometry and vertical excitation energies in reasonably large molecules such as those

examined here.[48] No provision for charge transfer is required in these computations because of the symmetry of the structures examined. Molecular orbital energies were also calculated at the same level of theory; those from HOMO-5 to LUMO+5 are reported.

The results reported here are those for which a C_{2v} symmetry constraint has been imposed on each of the full dimer structures. In order to examine the effects of potential geometric variations from C_{2v} in the dimer, calculations were also carried out on several dimers in which this constraint was lifted. In several instances, the unconstrained calculation automatically reproduced the constrained C_{2v} structure, and in all other cases examined the deviations from C_{2v} symmetry in the dimer was insignificant. Note that this C_{2v} constraint was applied only to the symmetric bis-porphyrin dimers; the individual monomeric units in the dimer exhibited significant departures from C_{2v} symmetry as noted in the data presented below. These results are similar to those found in a previous calculation on an axial ethynyl-linked tin porphyrin dimer.[42]

Time-dependent density functional theory has become one of the most promising and widely applied approaches for computing the excited state properties of medium sized to large scale molecular systems.[49-50] The TDDFT method can provide valence excited state geometries, excitation energies and transition oscillator strengths with the accuracy of more sophisticated quantum mechanical methods at low computational cost. In the present study, the vertical singlet and triplet electronic transition energies of the $(ZnP)_2X$ and $(ZnTriPP)_2X$ dimers have been predicted using the TD-B3LYP approach based upon the optimized ground state geometries *in vacuo*. All calculations were performed using the Gaussian 09 program.[51] The origin bands of the electronic absorption spectra have been simulated using the GaussSum program[53] with a half-bandwidth of 1500 cm^{-1}. Structural parameters have been calculated with the Mercury[54] program from the .mol files generated by Gaussian 09, which involve the 24-atom least squares mean planes of the two porphyrin rings.

The two ZnP dimers with the largest and the smallest interplanar spacings, $(ZnP)_2$DPS and $(ZnP)_2$DPB respectively, were selected for a further computational examination of the effects of solvation, the use of diffuse functions in the basis set and the inclusion of a dispersion function in the B3LYP functional. Full optimization at the B3LYP level of theory in the gas phase using the 6-31G(d) basis set was employed as the standard comparator for the geometries and vertical excitation spectra. The role of solvation was explored by using

benzene as a solvent and employing the polarizable continuum model (PCM)[55,56] of the self-consistent reaction field theory (SCRF) theory at the B3LYP/6-31G(d) level. To explore the role of including a diffuse function in the basis set, the two dimers were first optimized at the B3LYP level of theory in gas phase using the 6-31+G(d,p) basis set. The role of polarizability was then investigated by adding the D3 version of Grimme's dispersion function with the original D3 damping function.[57] Finally the combined effects of solvent, diffuse function and dispersion interaction were assessed by optimizing the two dimers at the B3LYP-D3/6-31+G(d,p) level of theory in benzene solvent employing the PCM model.

3. Results and Discussion:

The main structural parameters of the covalently linked dyads chosen for study are shown in Figure 1. Data sets were first generated for a monomeric unsubstituted ZnP species covalently bonded with another monomeric ZnP species using different rigid linkers (X = DPA, DPB, DPO, DPS and DPX), and imposing a C_{2v} symmetry constraint for the $(ZnP)_2X$ dimers. In order to examine the effects of peripheral *meso*-substitution, similar data sets were then generated for the triphenyl-*meso*-substituted macrocycles, ZnTriPP, covalently linked with the same rigid linkers to yield the corresponding $(ZnTriPP)_2X$ dimers.

3.1 Structural and Intra Dimer Parameters for Artificial Special Pairs

Structural and intra-dimer parameters for the ten covalently linked dimers and their respective monomers, generated initially by full optimization at the B3LYP level of theory in the gas phase using the 6-31G* basis set, are given in Tables 1 and 2. The macrocyclic centers (P_1 and P_2) are defined as the centers of the 4-N planes for each macrocycle. D_1 is the distance between the linker anchored carbon labeled 1 and the linker anchored carbon labeled 2 whereas D_2 is the distance between the linked *meso*-carbon atoms on the two macrocycles. The interplanar angle (β) is defined as the angle between the two macrocycle least-square planes. The slip angle ($\alpha=(\alpha_1+\alpha_2)/2$) is computed as the average angle between the vector joining the two macrocycle rings and the unit vectors normal to the two macrocycle least squares planes. For bis-porphyrins with large values of the interplanar angle, the slip angle will be approximately $\beta/2$. The lateral shift (D_7) is defined as $\sin(\alpha)\times D_5$[35] where D_5 is the P_1 to P_2 distance. Bond lengths and bond angles are shown in Table 1, and the intra-dimer parameters are given in Table 2. Each atom of the porphyrin rings and the linker is numbered in the standard fashion.

Trends in the bond lengths and angles of the macrocyclic core structures and the peripheral linkers are in general agreement with those observed experimentally in related systems.[26,27] The ten covalently linked dimers and their respective monomers confirm the imposed C_{2v} symmetry constraint (D_{4h} symmetry in the case of the ZnP monomer), but the monomeric units deviate from planarity when bonded in the dimers. The mean inter-planar separation is defined as D_6. In the dimers, each macrocycle is positioned in the plane formed by the four pyrrole nitrogen atoms (the 4-N structure), with the zinc atoms forced slightly out-of-plane. D_4, the vertical Zn atom out-of-plane displacement, exhibits an average mean value ranging from 0.008 Å for $(ZnP)_2DPX$ to 0.043 Å for $(ZnTriPP)_2DPX$. The average Zn-N bond length is 2.04 Å for all 12 structures including the monomers, in good agreement with X-ray crystallographic data.[26,27] The square geometry of the Zn core is confirmed by the average Zn-N_4 displacement of 0.022 Å and the average N-Zn-N bond angles of 90±0.3 degrees.

Three-dimensional views of the structures of the ten covalently linked dimers confirm the ability of all five rigid linkers to hold the two porphyrin rings in a cofacial arrangement. Significant intra-dimer parameters are summarized in Table 2. A semi-quantitative scheme previously used[58] to examine the effects of a pairwise overlap of the π systems of spatially oriented porphyrin monomers within a crystalline lattice provides a useful framework to analyze the structures of the linker-anchored porphyrin dimers described here. The most important intra dimer features of this aggregated dimer model are the interplanar angles, the lateral shifts of the metal centers and the mean separation of the macrocylic planes as defined above and footnoted in Table 2. In this model, authentic π-π interactions between aromatic macrocycles (as distinct from crystal packing effects) are signified by small lateral shifts (< 4Å). The data of Table 2 are unique in the way that lateral shifts have been collected for a homologous series of cofacial porphyrin dimers.

The variations in the *meso-meso* carbon distance (D_2), the P_1-P_2 distance (D_5), the mean plane separation (D_6) and other parameters also provide useful information when they are viewed as a function of linker structure. The D_2 distance (C-D, Figure 1) increases from DPB to DPS and follows the sequence DPB < DPX < DPA < DPO < DPS for both the $(ZnTriPP)_2X$ and $(ZnP)_2X$ dimers. The same sequence is also observed for the D_1, D_3, D_5 and D_6 distances, the smallest distance being always observed for the DPB linked dimer and the largest for the DPS linked dimer. There is little difference in this sequence for the D_5 and D_6 distances in the

$(ZnP)_2X$ dimers; these distances are almost equal for the DPB and DPX linked dimers. In contrast, the interplanar angle (β), slip angle (α) and lateral shift (D_7) are ordered in a similar sequence for DPB, DPO and DPS (DPB < DPO < DPS). However, for DPA and DPX a different sequence is observed for these same parameters; namely, DPX < DPA < DPB < DPO < DPS for both the $(ZnTriPP)_2X$ and $(ZnP)_2X$ dimer series. Only slight differences in the sequence are observed for the β and α angles in $(ZnTriPP)_2X$ dimers, where these angles differ by a small amount only for the DPA and DPX linked species. All these molecular structures confirm the ability of the rigid linkers to produce molecular clefts with a wide range of vertical pocket sizes. For the structures investigated here, the minimum inter-planar distance is found for the DPB linked dimer, which, not surprisingly, exhibits the strongest π-π interactions between the two porphyrin macrocycles.

3.2 Orbital Descriptions

In order to discuss the inter-porphyrin electronic interactions in these dimers, it is helpful to consider the properties of the molecular orbitals generated by population analysis, as shown in Table 3, again generated by full optimization at the B3LYP level of theory in the gas phase using the 6-31G* basis set. The addition of a second porphyrin ring results in a nearly additive geometric structure for the macrocycles of the dimer, but with varying inter-planar spacings and inter-planar angles. The electronic effects of situating the two porphyrin rings via different rigid linkers were therefore examined primarily by comparing the covalently linked dimers with the respective monomer. This comparison allows us examine the varying inter-macrocycle interactions which the rigid linkers enable. Table 3 illustrates that HOMO and HOMO-1 of a_{1u} and a_{2u} symmetry respectively in the monomeric D_{4h} ZnP molecule are represented by two pairs of MO's (HOMO to HOMO-3) with a_1, a_2, b_1 and b_2 symmetry in the C_{2v} dimers. The doubly degenerate LUMO of e_g symmetry in the ZnP monomer is correlated with four non-degenerate MO's (LUMO to LUMO +3) in the dimers. (Note that this doubly degenerate MO is labeled as LUMO and LUMO+1 in the subsequent tables in order to assist in correlating them with the same non-degenerate pair in the C_{2v} dimer structures.) Similarly, in the ZnTriPP monomer with C_{2v} symmetry, HOMO and HOMO-1 of b_1 and a_2 symmetry are split into four MO's (HOMO to HOMO-3) with a_1, a_2, b_1 and b_2 symmetry in the dimers. The pseudo-equiergic but non-degenerate LUMO and LUMO+1 in the ZnTriPP monomer are correlated with four non-degenerate MO's (LUMO to LUMO +3 again with a_1, a_2, b_1 and b_2 symmetry) in the dimers. This illustrates that a simple expansion

of Gouterman's four orbital model[43,44] to an eight-orbital model provides a satisfactory description of the frontier MOs for these porphyrin dimers. Note, however, that the rank order of the energies of HOMO to HOMO-3 and of LUMO to LUMO+3 is not followed by their symmetries from one dimer to another and this results in a similar disordering of the energies of the excited states belonging to each symmetry species.

All of these MOs are lowered in energy in the $(ZnTriPP)_2X$ dimers compared to the ZnTriPP monomer, with HOMO and LUMO exhibiting stabilizations of 0.19 to 0.08 eV and 0.09 to 0.01 eV respectively. HOMO and LUMO of the $(ZnP)_2X$ dimers compared with the ZnP monomer exhibit stabilizations of 0.29 to 0.06 eV and 0.12 to 0.01 eV respectively. Note that (i) the ZnP dimers generally exhibit greater HOMO and LUMO stabilizations than the ZnTriPP dimers, (ii) the stabilizations are greater in HOMO than LUMO resulting in a narrowing of the HOMO-LUMO gaps in the dimers, and (iii) within each set of five dimers the ones that have the smallest inter-planar spacings (X = DPB and DPX) produce the greatest effects, all as expected on the basis of exciton theory.

Figure 2 represents the frontier molecular orbitals of the two interacting macrocycles for the $(ZnTriPP)_2DPB$ dimer, which exhibits a modest excitonic splitting. The generated frontier orbitals exhibit clear atomic contributions from both macrocycles, indicating that the electron density of these MOs is shared over the two chromophores and that the coupled monomers act as a single entity. The convenient aspect of such a design is that this system is entirely and easily adjustable with respect to inter-planar angle, distance and slip by a simple change in linker.

3.3 Optical Absorption Spectra

The 75 lowest energy ground to excited state electronic transitions were calculated for each dimer using the TD-B3LYP method, again using the previously presented fully optimized structures *in vacuo*. Those that correlate with electronic transitions at energies up to and including the Soret-bands in the near UV-violet region were selected for analysis. Complete tables of these data (energies ≤ Soret) together with their corresponding oscillator strengths and one electron MO to MO promotion contributions to each transition are provided in the Supporting Information. Table 4 provides these data for selected representative dimers and a subset of the most important data for the others. (Note, however, that in documenting the MO to MO compositions of these transitions only contributions ≥ 10% of the total have been

included in Table 4.) Transitions at similar energies (i) to states of *gerade* parity in the D_{4h} ZnP monomer, (ii) to the corresponding pseudo-degenerate states of A_2 and B_1 symmetry in the C_{2v} ZnTriTPP monomer and (iii) to the states in the dimers that correlate with these forbidden or low intensity transitions in the monomers are also included in Table 4. Table 5 gives the calculated energies and symmetries of the triplet states corresponding to selected excited singlet states of the Q- and Soret-correlated bands, together with the orbital compositions of their spin-forbidden transitions. Figure 3 illustrates the effects of variations in the rigid linkers on the pure electronic spectra of the dyads; no vibronic transitions are shown. Figures 3a and 3b compare the predicted pure electronic absorption spectra of the $(ZnP)_2X$ and $(ZnTriPP)_2X$ dimers respectively with their monomers.

Two nearby porphyrinoids can interact electronically both by dipole-dipole coupling of their transition dipole moments and by direct mixing of their π orbitals. An example of the latter is provided in the recent computational report on porphyrin dyads coupled by short linkers that permit π electron delocalization.[59] Here, because the π systems of the macrocycles and the linkers are at right angles, the selected linkers provide no direct route for π electron delocalization via conjugation. Therefore the molecular exciton model has been used to provide the basic framework for understanding the calculated shifts and relative amplitudes of the electronic absorption bands in the dimers. To a first approximation, we can consider the dimers to be distorted H-aggregates, with distortions that increase with increasing values of the inter-planar angle, β. The smaller are β and the inter-planar spacing, D_6, the more likely the dimer is to behave like a strongly interacting face-to-face aggregate. The excitonic splittings should vary similarly. Using this scenario as a basis, we can expect to find two sets of splittings in the dimers. One of these will be associated with the removal of the degeneracy of LUMO in the ZnP monomers (denoted LUMO and LUMO+1 in the Tables), to match the existing near degeneracy of HOMO and HOMO-1. Removal of the pseudo-degeneracy of LUMO and LUMO+1 in the ZnTriPP monomer has the same effect in its dimers. The second effect will be the excitonic splitting caused by the inter-macrocycle interactions and this will be particularly evident in those dimers with small inter-planar spacings. Thus in the dimers there will be four MOs in the ground state (HOMO to HOMO-3) and four more in the excited state (LUMO to LUMO+3) involved in the transitions that correlate with the Q- and Soret-bands of the monomer. A total of 16 one electron MO to MO transitions is therefore expected

for each optical absorption in a dimer that corresponds to one arising from the four-orbital model in a D_{4h} monomer.

In a fully symmetric H-aggregate we would expect to see a blue-shift in the origin bands of the absorption spectra relative to the un-aggregated porphyrin because only the higher energy exciton-split state is reached from the ground state by an electric dipole allowed transition. TD-DFT calculations, however, enable us to see where both the parity forbidden and the red-shifted exciton-split bands would be if they could be observed in the experimental spectra of a fully symmetric D_{4h} dimer. Lifting the degeneracy (or near-degeneracy) of these frontier MOs in the C_{2v} dimers and the fact that the two interacting macrocycles are not parallel will also provide additional information in the computed spectra.

We employ the Mulliken convention in labeling the Cartesian axes in C_{2v}; z is the C_2 axis and y is parallel to the D_6 dimension in the dimer. The Q- and Soret-band transitions are in-plane polarized in the monomers, so the transition moments in the dimers are also expected to add vectorially to give a strong Soret- and a weak Q-band structure. In the dimers, the transition moments of the component macrocycles that are x polarized are parallel to one another and will add vectorially just as they do in the fully co-planar symmetric H-aggregate to give x polarized transitions terminating in excited states of B_1 symmetry. However the resultant transition moments that lie parallel to the C_2 axis and terminate in an excited state of A_1 symmetry are composed of the vector sums of macrocycle in-plane components of $\cos^2(\beta/2)$ fractional intensity and components of $\sin^2(\beta/2)$ fractional intensity that are directed perpendicular to each macrocycle plane in each dimer. In the symmetric dimer, the fractional intensities perpendicular to the C_2 axis and parallel to the y axis will be $\sin^2(\beta/2)\cos^2(\alpha)$. When the value of β is small this perpendicular component will contribute very little to the overall Q- or Soret-correlated band intensity in a dimer with large D_6.

Table 4 indicates that four of the lowest energy electron spin-allowed transitions in each dimer are composed of one-electron promotions between HOMO to HOMO-3 and LUMO to LUMO+3. There are 16 distinct one-electron promotions in total, with each transition in the set of four composed of four one-electron MO to MO promotions each of which contributes approximately ¼ of the calculated intensity. The oscillator strengths are all small because the Q bands arise from the vector addition of opposed transition moments of nearly equal

magnitude in each monomer. The variations from dimer to dimer in the computed oscillator strengths of these low energy transitions are therefore strongly influenced by the separation between HOMO and HOMO-1 in the ZnP dimers and between the pairs of HOMO, HOMO-1 and HOMO-2, HOMO-3 in the ZnTriPP dimers. In all the dimers investigated, these low energy one-electron promotions may be grouped into sets of four, with one upper state of each C_{2v} symmetry species in each set. The data of Table 4 indicate that all of these pure electronic transitions are of low oscillator strength, but that those of z and x polarization and terminating in the A_1 and B_1 states, respectively, are the strongest and of the highest energy. Transitions to the A_2 states are all electric dipole forbidden, as required. In the dimers with larger inter-planar angles and smaller inter-planar spacings, a weaker transition to an excited state of B_2 symmetry appears in this same energy region, corresponding to the y-polarized component of the opposed vector addition.

If the above analysis is correct, we should expect to find a corresponding set of four electronic spin-allowed transitions at higher energy that correlate with the split Soret bands in the coupled monomers. This is generally true, except that in this higher energy region the contributions of one-electron MO to MO promotions from orbitals lower in energy than HOMO-3 and higher in energy than LUMO+3 are significant in some cases. HOMO-4 and LUMO+4 appear most frequently, and when they do the percentage contributions of the one electron MO to MO promotions can differ considerably from the approximately 25% contributions found in the Q-band energy region. The extent to which these additional one electron MO to MO promotions contribute to the intensity in the Soret-correlated region increases as the degree of interaction between the two component macrocycles increases. Nevertheless, the same basic structure is apparent, with the electronic transitions to the A_1 and B_1 states located at the highest energies and exhibiting the largest oscillator strengths (f of the order of 1 or more). The y polarized transitions to the B_2 excited state can have considerable intensity in this region, with values of f that approach those of the x polarized transitions in the DPO and DPS dimers with large inter-planar angles.

The expected blue shifts in the strong Soret bands of the dimers compared with their constituent monomers are observed, but the splitting between the two strongest z- and x-polarized bands remains relatively small. More detail is discernible as the linker and constituent porphyrin are varied. For the $(ZnP)_2X$ dimers investigated here, the Soret blue-shift shift is about 7 nm (Table 4) relative to the respective monomer (ZnP) depending on the

slip angle; the larger the slip angle, the smaller the blue shift, as expected. For the $(ZnTriPP)_2X$ dimers this shift is about 5 nm (Table 4) relative to the respective monomer (ZnTriPP), again depending on the slip angle. The Soret band shift in the covalently linked dimers (relative to the respective monomers) is also a function of the mean plane separation, D_6. The Soret bands of the $(ZnP)_2X$ dimers exhibit increasing blue shifts (in comparison to their ZnP monomer) with decreasing mean plane separation. Consistent with this trend, triphenyl substitution of the porphyrin monomer results in a set of smaller blue shifts in the Soret transitions of the dimers due to the incremental increase in D_6 resulting from inter-substituent crowding.

Additional weak pure electronic transitions from the ground state to the lower-lying excitonic states are also expected to appear in the computed spectra of the dimers. Eight such transitions, consisting of two sets of four, can be identified in the region between the Q- and Soret-correlated transitions. As a group they contain all 16 distinct one-electron MO to MO contributions expected from the eight participating MOs. All of these computed pure electronic transitions are of low intensity but the strongest among them are z- and y-polarized, terminating in states of A_1 and B_2 symmetry respectively.

Additional transitions largely involving single one-electron promotions most frequently originating in HOMO-4, HOMO-5, HOMO-6, … and terminating in LUMO to LUMO+3 or originating in HOMO to HOMO-3 and terminating in LUMO+4 are also found at energies slightly lower than or overlapping with the Soret-correlated transitions. These are easy to identify and are correlated with transitions that are either (i) parity forbidden in the D_{4h} ZnP monomer or (ii) of low intensity from HOMO-2 to the non-degenerate LUMO and LUMO+1 in the C_{2v} ZnTriPP monomer. They do not exhibit large values of f, but the strongest of them are either z or y polarized, terminating in excited states of A_1 or B_2 symmetry respectively.

These data can now be used to interpret the experimentally measured UV-visible absorption spectra of artificial special pairs previously reported in the literature. The UV-visible spectra of molecules structurally similar to $(ZnP)_2DPB$[32] and the other ZnP dimers,[34] and to $(ZnTriPP)_2DPS$[37] have been measured but no details of their interpretation other than a broad assignment of features to the Q- and Soret-bands have been provided. We now see that a relatively strong band that appears as a shoulder on the red side of the very strong Soret features in many of these molecules can be assigned to the y polarized electric dipole-allowed

transition to the B_2 Soret-correlated state that is particularly evident in the dimers with large inter-planar angles. This band also appears in polymers containing pendant zinc porphyrin substituents,[60] and contributes to the absorption to the red of the Soret band maxima in surface active zinc porphyrins in Langmuir-Blodgett films.[61] Although no excitonic splittings can be seen in the solution phase spectra, the blue shift of the Soret bands relative to the monomers and the observed broadening of the prominent features corresponding to the Soret transitions in these cofacial bis-porphyrins can now be interpreted in terms of excitonic coupling of the two macrocycles.

Many pure electronic transitions of low intensity are computed to lie between the observed strong Soret and Q-bands of the dimers. These may contribute to a widening of the observed bands in the solution spectra, but are obscured by the vibronic structure that appears in this energy region. Nevertheless, the presence of these electronic states is expected to significantly influence the rates and mechanisms of excited state relaxation for these dimers when excited in their strong absorption bands in the near UV-violet region.

3.4 Effects of solvation, expanded basis set and diffuse function

Table 5 compares the effects on the calculated B3LYP/6-31G(d) structural parameters of the $(ZnP)_2$DPB and $(ZnP)_2$DPS dimers (column 1, reproduced from Table 2) resulting from: solvating with benzene using the polarizable continuum model (column 2), adding diffuse functions to the basis set (column 3), adding the Grimme dispersion function to the B3LYP functional (column 4), and including all of solvation, diffuse functions and dispersion (column 5). As anticipated, the effects are greatest for the $(ZnP)_2$DPB dimer, which by virtue of its linker has the smallest interplanar spacing and interplanar angle and are much smaller for the $(ZnP)_2$DPS dimer. However, none of these incremental effects alters the conclusions drawn from the lower level *in vacuo* calculations reported in Tables 1 and 2. Calculations of the HOMO and LUMO energies and the vertical Q and Soret band energies using the corresponding TD-B3LYP protocols for these two dimers are also reported in Taable 5. The inclusion of dispersion in the functionals has the expected effect of lowering the MO energies and producing a significantly greater red-shift in the Soret optical excitation energies, thereby more closely approximating the experimental data.[32,34,37]

3.5 Triplet states

The energies and symmetries of the triplet states of the monomers and ten dimers are listed in Table 6, together with the orbital compositions of their spin-forbidden one-photon transitions to the ground state. Only data for the lowest two triplet states of the monomers and the corresponding eight triplet states of the ten dimers are listed. Comparing the triplet states of the dimers with those of the respective monomers, one observes a relatively modest effect of macrocyclic interactions in the dimer. The correlated triplet states in the dimer are located only about 0.05 eV higher than T_1 in the monomer, whereas a difference of about 0.02 eV is found in the Soret-correlated triplets derived from T_2 in the monomer. Since the exciton splitting depends upon the oscillator strength of the transition, only the singlet states of the dimers are split to a measurable extent. The triplet states of the dimer remain nearly degenerate.

4. Conclusion:

Time-dependent density functional theory investigations show that significant inter-macrocyclic interactions are introduced when two porphyrins are linked covalently via a rigid linker in a cofacial arrangement. The dyads are predicted to behave spectroscopically similar to distorted H-aggregates. The expansion of Gouterman's four orbital approach for the monomer to an eight orbital approach in the dimer produces a satisfactory framework for analyzing the computational data and for interpreting the spectra of structurally similar cofacial bis-porphyrins.

5. Acknowledgements:

The authors are pleased to acknowledge the continuing support of this research by the Natural Sciences and Engineering Research Council of Canada. This research has been enabled by the use of computing resources provided by WestGrid and Compute/Calcul Canada. NA thanks the Department of Science and Technology (India) for an INSPIRE faculty award.

6. References:

1. S. Karrasch, P.A. Bulloughand R. Ghosh, *EMBO J.*, 1995,**14**, 631.
2. J. Koepke, X. Hu, C. Muenke, K. Schultenand H. Michel, *Structure*, 1996, **4**, 581.
3. G. McDermott, S.M. Prince, A.A. Freer, A.M. Hawthornthwaite-Lawless,M.Z. Papiz,R.J. Cogdelland N.W. Isaacs, *Nature,*1995, **374**, 517.
4. K. McLuskey, S.M. Prince, R.J. Cogdelland N.W. Isaacs, *Biochemistry,* 2001, **40**, 83.

5. H. Savage, M. Cyrklaff, G. Montoya,W. Kuhlbrandtand I. Sinning, *Structure,* 1996, **4**, 243.
6. T.Walz, S.J. Jamieson, C.M. Bowers, P.A. Bulloughand C.N. Hunter, *J. Mol.Biol.,* 1998, **282,** 833.
7. A.W. Roszak, T.D. Howard, J. Southall, A.T. Gardiner, C.J. Law, N.WIsaacsand R.J. Cogdell, *Science,* 2003, **302,** 1969.
8. G. Feher, A.l. Hoff, R.A. Isaacson and L.E. Ackerson, *Ann. N.Y. Acad. Sci.,* 1975, **244**, 239.
9. J.R. Norris, R.A. Uphaus, R.L. Crespi and J.J. Katz, *Proc. Nat. Acad. Sci. USA,*1971, **68**, 625.
10. J. Fajer, M.S. Davis, D.C. Brune, L.D. Spaulding, D.E. Borg and A. Forman,*Brookhaven Symp. BioI. Chlorophyll-Proteins, Reaction Centers and Photosynthetic Membranes*, 1977, 74.
11. J.J. Katz. J.R. Norris. L.L. Shipman, M.E. Thumauer and M.R. Wasielewski, *Ann. Rev. Biophys. Bioeng.,*1978, **7,** 393
12. R.S. Selensky, D. Holten, M.W. Windsor, J.B. Paine III and D. Dolphin, *Chem. Phys.*, 1981, **60**, 33.
13. B.R. Green and W.W. Parson, Advances in Photosynthesis and Respiration, in *Light Harvesting Antennas in Photosynthesis,* Kluwer Academic Publishers, 2003, vol. 13.
14. P.D. Harvey in*The Porphyrin Handbook,*K.M. Kadish, K.M. Smith, R. Guilard (Eds.),vol. 18, Academic Press, San Diego,2003, pp. 63–250, and references therein.
15. X. Peng, N. Aratani, A. Takagi, T. Matsumoto, T. Kawai, I.-W. Hwang,T.K. Ahn, D. Kim, A. Osuka, *J. Am. Chem. Soc.,* 2004, **126**, 4468.
16. R. Takahashi, and Y. Kobuke, *J. Am. Chem. Soc.,* 2003, **125,** 2372.
17. D. Kim, and A. Osuka, *Acc. Chem. Res.,* 2004, **37,** 735.
18. P.D. Harvey, C. Stern and R. Guilard in *Bioinspired Molecular Devices in Photosynthetic Bacteria*, Handbook of Porphyrins and Phthalocyanines, K. Kadish, R. Guilard and K. M. Smith,Eds.,vol. 11, World Science, 2011,p. 1.
19. P.D. Harvey, *Can. J. Chem.,* 2014, **92**, 355.
20. P.D. Harvey, C. Stern, C.P. Gros and R. Guilard, *Coord. Chem. Rev.* 2007, **251**,401.
21. J.P. Fillers, K.G. Ravichandran, I. Abdalmuhdi, A. Tulinsky and C.K. Chang, *J. Am. Chem. Soc.* 1986, **108**, 417.
22. S.S. Eaton, G.R. Eaton and C.K. Chang, *J. Am Chem. Soc.,*1985, **107**, 3177.
23. C.K. Chang and I. Abdalmuhdi, *J. Org. Chem.*, 1983, **48**, 5388.

24. C.K. Chang and I. Abdalmuhdi, *Angew. Chem. Int. Ed. Engl*.,1984, **23**, 164.
25. Y. Deng, C.J. Chang, and D.G. Nocera, *J. Am. Chem. Soc.,* 2000, **122**, 410.
26. C.J. Chang, E.A. Baker, B.J. Pistorio, Y. Deng, Z.-H. Loh, S.E. Miller, S.D. Carpenter and D.G. Nocera, *Inorg. Chem.* 2002, **41**, 3102.
27. C.J. Chang, Y. Deng, A.F. Heyduk, C.K. Chang and D.G. Nocera, *Inorg. Chem.* 2000, **39**, 959.
28. P.D. Harvey, C. Stern, C.P. Gros and R. Guilard, *J. Porphyrins Phthalocyanines,* 2010, **14**, 55.
29. J.-M. Camus, A. Langlois, S.M. Aly and R. Guilard, *Chem. Commun.*, 2013, **49**, 2228.
30. A. Takai, C.P. Gros, J.-M. Barbe, R. Guilard and S. Fukuzumi, *Chem., Eur. J.*, 2009, **15**, 3110.
31. P.D. Harvey, F. Brégier, S.M. Aly, J. Szmytkowski, M.F. Paige and R.P. Steer, *Chem. Eur. J.,* 2013, **19**, 4352.
32. J.-M. Camus, S.M. Aly, C. Stern, R. Guilard and P.D. Harvey, *Chem. Commun.,* 2011, **47**, 8817.
33. P.D. Harvey,A. Langlois, M. Filatov, D. Fortin, K. Ohkubo, S. Fukuzumi andR. Guilard, *J. Porphyrins Phthalocyanines,* 2012, **16**, 685.
34. S. Faure, C. Stern, R. Guilard and P.D. Harvey, *J. Am. Chem. Soc.,* 2004, **126**, 1253.
35. F. Brégier, S.M. Aly, C.P. Gros, J.-M. Barbe, Y. Rousselin and P.D. Harvey, *Chem. Eur. J.,* 2011, **17**, 14643.
36. P.D. Harvey, N. Proulx, G. Martin, M. Drouin, D.J. Nurco, K.M. Smith, F. Bolze, C.P. Gros and R. Guilard, *Inorg. Chem.,* 2001, **40**, 4134.
37. S. Faure, C. Stern, R. Guilard and P.D. Harvey, *Inorg. Chem.,* 2005, **44**, 9232.
38. P.D. Harvey, M.A. Filatov and R. Guilard, *J. Porphyrins Phthalocyanines*, 2011, **15**, 1150.
39. C.P. Gros, F. Brisach, A. Meristoudi, E. Espinosa, R. Guilard and P.D. Harvey, *Inorg. Chem.,* 2007, **46**, 125.
40. F. Bolze, M. Drouin, P.D. Harvey, C.P. Gros, E. Espinosa and R. Guilard, *J. Porphyrins Phthalocyanines,* 2003, **7**, 474.
41. F. Bolze, C.P. Gros, M. Drouin, E. Espinosa, P.D. Harvey and R. Guilard, *J. Organomet. Chem.*, 2002, **643-644**, 89.
42. N. Agnihotri and R.P. Steer, *J. Porphyrins Phthalocyanines,* 2015, **19**, 610.
43. M. Gouterman, *J. Mol. Spectrosc.* 1961, **6**, 138.

44. M. Gouterman, G. Wagniere and L.C. Snyder, *J. Mol. Spectrosc.* 1963, **11**, 108.
45. A.D. Becke, *Phys. Rev. A,* 1988, **38,** 3098.
46. C.T. Lee, W.T. Yangand R.G. Parr, *Phys. Rev. B,* 1988, **37,** 785.
47. A.D. Becke, *J. Chem. Phys.,*1993, **98,** 5648.
48. K.A. Nguyen and R. Pachter: *J. Chem. Phys.,* 2001, **114,** 10757.
49. R.E. Stratmann, G.E. Scuseriaand M.J. Frisch, *J. Chem. Phys.,*1998, **109,** 8218.
50. R. Bauernschmittand R. Ahlrichs, *Chem. Phys. Lett.,*1996, **256,** 454.
51. M.E. Casida, C. Jamorski, K.C. Casidaand D.R. Salahub, *J. Chem. Phys.,*1998, **108,**4439.
52. M.J. Frisch *et al*., *GAUSSIAN 09 (Revision D.01),* Gaussian, Inc., Wallingford CT, 2013.
53. N.M. O'Boyle, A.L. Tenderholt and K.M. Langner. *J. Comp. Chem.* 2008, **29**, 839.
54. C.F. Macrae, I.J. Bruno, J.A. Chisholm, P.R. Edgington, P. McCabe, E. Pidcock, L. Rodriguez-Monge, R. Taylor, J. van de Streek and P.A. Wood, *J. Appl. Cryst.,* 2008, **41**, 466.
55. S. Miertus, E. Scrocco and J. Tomasi, *Chem. Phys.* 1981, **55**, 117.
56. M. Cossi, G. Scalmani, N. Rega and V. Barone, *J. Chem. Phys.* 2002, **117**, 43.
57. S. Grimme, J. Antony, S. Ehrlich and H. Krieg, *J. Chem. Phys*., 2010, **132**, 154104.
58. W.R. Scheidtand Y. J. Lee, *Struct*. *Bonding* (*Berlin*) 1987, **64**, 1.
59. L. Rintoul, S.R. Harper and D.P. Arnold, *Phys. Chem. Chem. Phys.,* 2013, **15**, 18951.
60. S. Novakovic, W.W.H. Wong, K.P. Ghiggino and R.P. Steer, unpublished data.
61. C.P. Ponce, H.Y. Araghi, N.K. Joshi, R.P. Steer and M.F. Paige, *Langmuir*, 2015,**31**, 13590.

Figures:

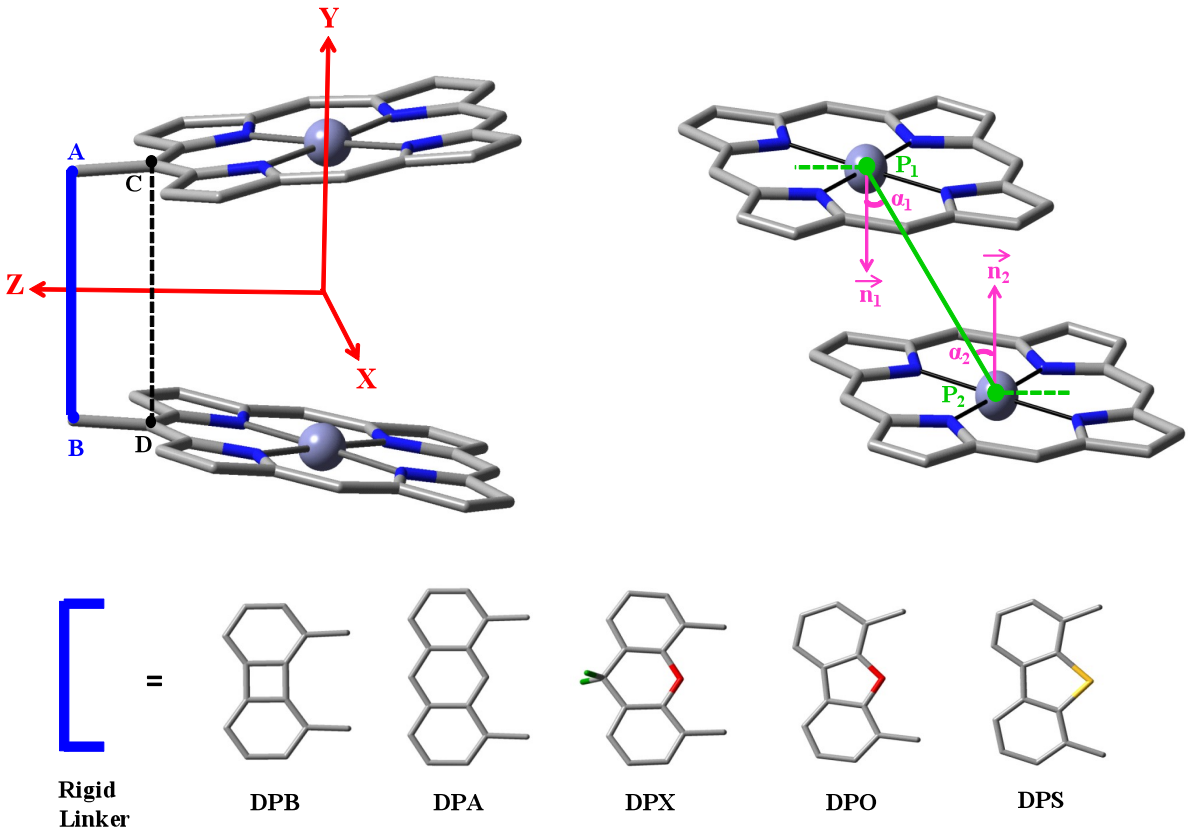

Figure 1: Schematic diagram of the rigid structures covalently linking two porphyrin monomers (ZnP or ZnTriPP) to form the cofacial bisporphyrin dimers explored here. The hetero-atoms in DPX, DPO and DPS are O, O and S respectively. The A-B and C-D distances are defined in Table 2 for each set of dimers. P_1 and P_2 are the two macrocycle centers with normal vectors n_1 and n_2, and α_1 and α_2 are the slip angles, which are also defined in detail in the text and Table 2.

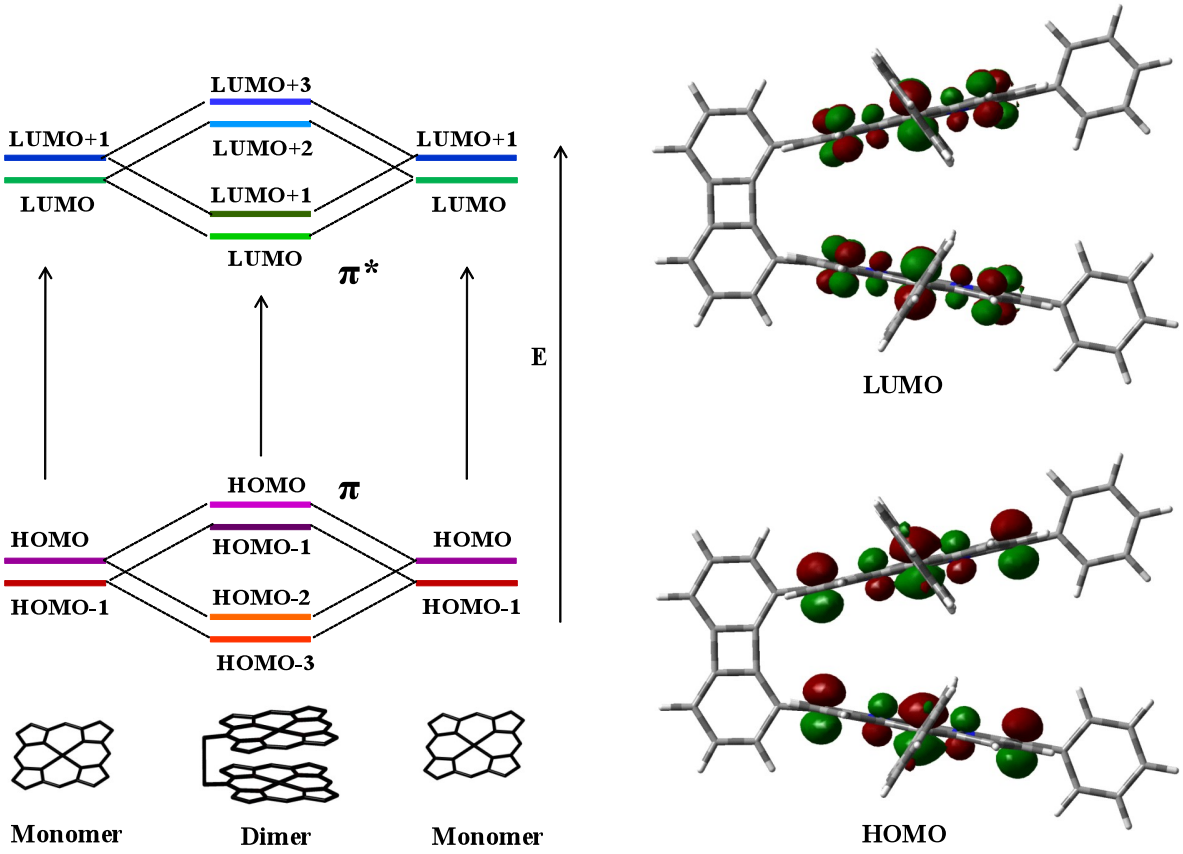

Figure 2: Left: Simplified MO model (not to scale) illustrating the effect of π-π stacking of the two interacting porphyrins on the HOMO-LUMO cluster and the expansion of Gouterman's four orbital model to an eight orbital approach. Right: Representations of the frontier MOs in an optimized geometry (B3LYP/6-31G(d) level) for a cofacial $(ZnTriPP)_2DPB$ dimer.

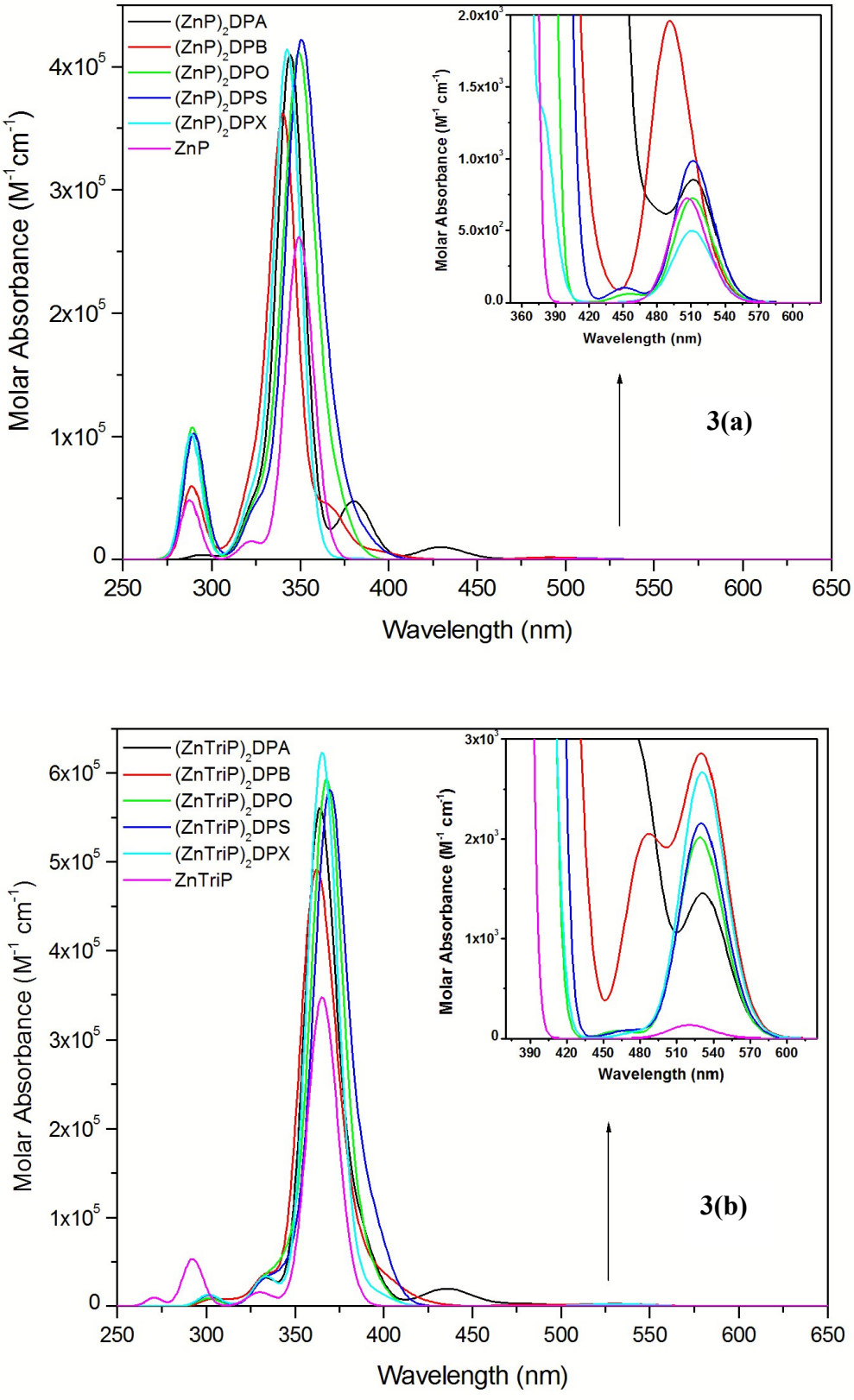

Figure 3: Simulated absorption spectra of $(ZnP)_2X$ and $(ZnTriPP)_2X$, where (X = DPA, DPB, DPO, DPS, DPX), obtained at the TD-B3LYP/6-31G(d) level of theory *in vacuo* with a C_{2v} symmetry constraint.

Table 1: Geometrical parameters of the dimers $(ZnP)_2X$ and $(ZnTriPP)_2X$, where (X = DPA, DPB, DPO, DPS, DPX), obtained at the B3LYP/6-31G(d) level of theory *in vacuo* with a C_{2v} symmetry constraint.

Bond Lengths (Å)	**ZnP (D_{4h})**	**$(ZnP)_2$ DPA**	**$(ZnP)_2$ DPB**	**$(ZnP)_2$ DPO**	**$(ZnP)_2$ DPS**	**$(ZnP)_2$ DPX**	**ZnTriPP**	**$(ZnTriPP)_2$ DPA**	**$(ZnTriPP)_2$ DPB**	**$(ZnTriPP)_2$ DPO**	**$(ZnTriPP)_2$ DPS**	**$(ZnTriPP)_2$ DPX**
Zn_1-N_1	2.042	2.043	2.044	2.044	2.040	2.044	2.043	2.042	2.043	2.043	2.042	2.044
Zn_1-N_2	2.042	2.043	2.044	2.044	2.040	2.044	2.043	2.042	2.043	2.043	2.042	2.044
Zn_1-N_3	2.042	2.041	2.040	2.040	2.044	2.040	2.039	2.042	2.041	2.041	2.042	2.041
Zn_1-N_4	2.042	2.041	2.040	2.040	2.044	2.040	2.039	2.042	2.041	2.041	2.042	2.041
Zn_2-N_5	----	2.043	2.044	2.044	2.040	2.044	----	2.042	2.043	2.043	2.042	2.044
Zn_2-N_6	----	2.043	2.044	2.044	2.040	2.044	----	2.042	2.043	2.043	2.042	2.044
Zn_2-N_7	----	2.041	2.040	2.040	2.044	2.040	----	2.042	2.041	2.041	2.042	2.041
Zn_2-N_8	----	2.041	2.040	2.040	2.044	2.040	----	2.042	2.041	2.041	2.042	2.041
Bond Angles (deg.)												
N_1-Zn_1-N_2	90	89.64	89.61	89.62	89.63	89.63	90.59	90.25	90.26	90.19	90.22	90.27
N_1-Zn_1-N_3	90	90.54	90.51	90.50	90.51	90.52	89.51	89.77	89.71	89.77	89.75	89.70
N_2-Zn_1-N_3	180	179.10	179.34	178.72	179.17	179.51	179.89	178.61	177.94	178.71	179.15	177.60
N_1-Zn_1-N_4	180	179.10	179.34	178.72	179.17	179.51	179.89	178.61	177.94	178.71	179.15	177.60
N_2-Zn_1-N_4	90	90.54	90.51	90.50	90.51	90.52	89.51	89.77	89.71	89.77	89.75	89.70
N_3-Zn_1-N_4	90	89.27	89.36	89.36	89.34	89.32	90.38	90.18	90.25	90.25	90.26	90.24
N_7-Zn_2-N_8	----	89.27	89.36	89.36	89.34	89.32	----	90.18	90.25	90.25	90.26	90.24
N_7-Zn_2-N_6	----	179.10	179.34	178.72	179.17	179.51	----	178.61	177.94	178.71	179.15	177.60
N_8-Zn_2-N_6	----	90.54	90.51	90.50	90.51	90.52	----	89.77	89.71	89.77	89.75	89.70
N_7-Zn_2-N_5	----	90.54	90.51	90.50	90.51	90.52	----	89.77	89.71	89.77	89.75	89.70
N_8-Zn_2-N_5	----	179.10	179.34	178.72	179.17	179.51	----	178.61	177.94	178.71	179.15	177.60
N_6-Zn_2-N_5	----	89.64	89.61	89.62	89.63	89.63	----	90.25	90.26	90.19	90.22	90.27

Table 2: Intra-dimer geometrical parameters for $(ZnP)_2X$ and $(ZnTriPP)_2X$, where (X = DPA, DPB, DPO, DPS, DPX) obtained at the B3LYP/6-31G(d) level of theory *in vacuo* with a C_{2v} symmetry constraint.

Parameters	**$(ZnP)_2$ DPA**	**$(ZnP)_2$ DPB**	**$(ZnP)_2$ DPO**	**$(ZnP)_2$ DPS**	**$(ZnP)_2$ DPX**	**$(ZnTriPP)_2$ DPA**	**$(ZnTriPP)_2$ DPB**	**$(ZnTriPP)_2$ DPO**	**$(ZnTriPP)_2$ DPS**	**$(ZnTriPP)_2$ DPX**
D_1 (A-B) Distance[a] (Å)	4.987	3.842	4.848	5.281	4.710	5.000	3.869	4.850	5.283	4.736
D_2 (C-D) Distance[b] (Å)	5.089	3.970	5.580	6.392	4.558	5.205	4.142	5.595	6.411	4.747
D_3 (Zn(1)-Zn(2)) Distance[c] (Å)	5.327	4.433	7.299	8.958	4.438	6.105	5.434	7.295	9.025	5.593
D_4(Zn-N_4) Av. Displacement[d] (Å)	0.016	0.011	0.023	0.015	0.008	0.025	0.037	0.023	0.015	0.043
D_5 (P_1-P_2) Distance[e] (Å)	5.358	4.456	7.343	8.984	4.455	6.154	5.506	7.340	9.054	5.677
D_6 Mean Plane Separation[f] (Å)	5.359	4.466	7.104	8.344	4.460	6.123	5.460	7.104	8.350	5.684
βInterplanarAngle[g] (°)	4.37	7.77	29.55	43.58	1.13	16.82	23.31	29.57	45.65	16.92
α Slip Angle[h] (°)	1.92	3.83	14.78	21.79	1.21	8.38	11.66	14.78	22.83	8.49
D_7Lateral Shift[i] (Å)	0.18	0.30	1.87	3.33	0.09	0.90	1.11	1.87	3.51	0.84

[a]Distance between the linker anchored carbon 1 and the linker anchored carbon 2.
[b]Distance between the *meso* carbon 1 and *meso* carbon 2 atoms on the porphyrin macrocycles.
[c]Distance between the two Zn atoms in the dimer.
[d]Average displacement of the Zn atom from the centroids of the 4-Nitrogen planes in each macrocycle.
[e]Distance between the centroids of the 4-Nitrogen planes in each macrocycle.
[f]The plane separation is defined as the perpendicular distance from one macrocycle's 24-atom least-squares plane to the centroid of the 24-atom least-squares plane of the other macrocycle; the mean plane separation is the average of the two plane separations.
[g]The interplanar angle (β) is the angle between the two macrocyclic 24-atom least square planes.
[h]The slip angle ($\alpha = (\alpha_1+\alpha_2)/2$) is the average angle between the vector joining the two 24-atom macrocyclic centroids and the unit vectors normal to the two 24-atom least square planes.
[i]Lateral shift is defined as $[\sin(\alpha)\times D_5]$.

Table 3: Molecular orbital energies (in eV) of $(ZnP)_2X$ and $(ZnTriPP)_2X$, where (X = DPA, DPB, DPO, DPS, DPX), obtained at the B3LYP level of theory with a 6-31G(d) basis set *in vacuo* with a C_{2v} symmetry constraint.

Orbitals	**ZnP (D_{4h})**		**$(ZnP)_2$ DPA**		**$(ZnP)_2$ DPB**		**$(ZnP)_2$ DPO**		**$(ZnP)_2$ DPS**		**$(ZnP)_2$ DPX**		**ZnTriPP**		**$(ZnTriPP)_2$ DPA**		**$(ZnTriPP)_2$ DPB**		**$(ZnTriPP)_2$ DPO**		**$(ZnTriPP)_2$ DPS**		**$(ZnTriPP)_2$ DPX**	
	Sym	**E(eV)**	**Sym**	**E(eV)**	**Sym**	**E(eV)**	**Sym**	**E(eV)**	**Sym**	**E(eV)**	**Sym**	**E(eV)**	**Sym**	**E(eV)**	**Sym**	**E(eV)**	**Sym**	**E(eV)**	**Sym**	**E(eV)**	**Sym**	**E(eV)**	**Sym**	**E(eV)**
HOMO-5	$4e_g$	-6.60	$44a_2$	-6.23	$43a_2$	-6.20	$45b_1$	-6.17	$44a_2$	-6.11	$44a_2$	-6.14	$14a_2$	-6.49	$67a_2$	-6.20	$66a_2$	-6.18	$68b_1$	-6.12	$67a_2$	-6.05	$67a_2$	-6.14
HOMO-4	$4e_g$	-6.60	$45b_1$	-5.33	$44a_2$	-5.47	$44a_2$	-6.09	$46b_1$	-5.79	$46b_1$	-5.68	$24b_1$	-6.48	$68b_1$	-5.31	$67a_2$	-5.44	$67a_2$	-6.04	$69b_1$	-5.74	$68b_1$	-5.68
HOMO-3	$2b_{2u}$	-6.59	$74a_1$	-5.10	$71a_1$	-5.14	$46b_1$	-5.12	$70b_2$	-5.18	$74a_1$	-5.07	$15a_2$	-6.44	$68a_2$	-5.06	$68b_1$	-5.09	$69b_1$	-5.07	$68a_2$	-5.09	$69b_1$	-5.02
HOMO-2	$10b_{1g}$	-6.35	$45a_2$	-5.08	$45b_1$	-5.14	$72a_1$	-5.12	$74a_1$	-5.16	$47b_1$	-5.07	$49b_2$	-6.26	$69b_1$	-4.99	$68a_2$	-5.01	$68a_2$	-5.06	$70b_1$	-5.09	$68a_2$	-5.00
HOMO-1	$5a_{2u}$	-5.22	$70b_2$	-5.08	$45a_2$	-4.97	$69b_2$	-5.12	$45a_2$	-5.15	$45a_2$	-4.93	$16a_2$	-5.14	$111a_1$	-4.97	$107a_1$	-4.97	$109a_1$	-4.98	$107b_2$	-5.01	$111a_1$	-4.91
HOMO	$1a_{1u}$	-5.21	$46b_1$	-5.04	$68b_2$	-4.97	$45a_2$	-5.11	$47b_1$	-5.15	$70b_2$	-4.92	$25b_1$	-5.08	$107b_2$	-4.97	$105b_2$	-4.91	$106b_2$	-4.97	$111a_1$	-5.00	$107b_2$	-4.89
LUMO	$5e_g$	-2.14	$75a_1$	-2.07	$72a_1$	-2.09	$73a_1$	-2.08	$71b_2$	-2.13	$75a_1$	-2.02	$17a_2$	-2.10	$69a_2$	-2.06	$69b_1$	-2.10	$110a_1$	-2.06	$108b_2$	-2.10	$70b_1$	-2.01
LUMO+1	$5e_g$	-2.14	$71b_2$	-2.04	$46b_1$	-2.09	$70b_2$	-2.08	$75a_1$	-2.13	$48b_1$	-2.00	$26b_1$	-2.10	$112a_1$	-2.06	$108a_1$	-2.08	$70b_1$	-2.06	$112a_1$	-2.09	$112a_1$	-2.01
LUMO+2	$2b_{1u}$	-0.54	$47b_1$	-2.03	$69b_2$	-1.94	$47b_1$	-2.06	$46a_2$	-2.10	$71b_2$	-1.90	$27b_1$	-0.50	$108b_2$	-2.05	$69a_2$	-2.01	$107b_2$	-2.06	$69a_2$	-2.08	$69a_2$	-2.00
LUMO+3	$6a_{2u}$	0.86	$46a_2$	-2.02	$46a_2$	-1.92	$46a_2$	-2.05	$48b_1$	-2.09	$46a_2$	-1.88	$50b_2$	-0.11	$70b_1$	-2.05	$106b_2$	-1.99	$69a_2$	-2.05	$71b_1$	-2.08	$108b_2$	-1.98
LUMO+4	$16a_{1g}$	1.19	$48b_1$	-1.71	$47b_1$	-1.28	$48b_1$	-1.02	$49b_1$	-1.01	$49b_1$	-0.45	$66a_1$	-0.09	$71b_1$	-1.69	$70b_1$	-1.25	$71b_1$	-0.97	$72b_1$	-0.96	$113a_1$	-0.47
LUMO+5	$3b_{2u}$	1.36	$76a_1$	-0.46	$48b_1$	-0.83	$74a_1$	-0.48	$76a_1$	-0.52	$76a_1$	-0.43	$51b_2$	-0.05	$113a_1$	-0.50	$71b_1$	-0.80	$111a_1$	-0.49	$113a_1$	-0.52	$71b_1$	-0.45
HOMO-LUMO Gap (eV)	**3.07**		**2.97**		**2.88**		**3.03**		**3.02**		**2.90**		**2.98**		**2.91**		**2.81**		**2.91**		**2.90**		**2.88**	

Table 4: Excitation energies (in eV), oscillator strengths (f) and one electron MO to MO compositions of the electronic transitions to singlet excited states in the dimers $(ZnP)_2X$ and $(ZnTriPP)_2X$, where (X = DPA, DPB, DPO, DPS, DPX), obtained at the TD-B3LYP/6-31G(d) level of theory *in vacuo* with a C_{2v} symmetry constraint.

States	Composition of Transitions										E(eV)	f
ZnP												
S1(1^1E_u)	H→L	50%	H-1→L+1	49%							2.45	0.0025
S2(1^1E_g)	H-2→L+1	100%									3.34	0.0000
S3(2^1E_u)	H-1→L+1	46%	H→L	48%							3.55	0.9024
$(ZnP)_2$DPA												
S1(1^1A_2)	H-3→L+3	20%	H-2→L	24%	H-1→L+2	25%	H→L+1	29%			2.41	0.0000
S2(1^1B_2)	H-3→L+1	21%	H-2→L+2	23%	H-1→L	28%	H→L+3	26%			2.41	0.0000
S3(1^1B_1)	H→L	33%	H-1→L+3	23%	H-3→L+2	23%	H-2→L+1	20%			2.41	0.0049
S4(1^1A_1)	H→L+2	29%	H-1→L+1	25%	H-3→L	24%	H-2→L+3	20%			2.41	0.0008
S5(2^1B_1)	H→L	49%	H-2→L+1	47%							2.58	0.0002
S6(2^1A_2)	H-2→L	45%	H→L+1	53%							2.58	0.0000
S7(2^1B_2)	H→L+3	49%	H-2→L+2	39%							2.61	0.0018
S8(2^1A_1)	H→L+2	46%	H-2→L+3	46%							2.61	0.0016
S9(3^1A_1)	H-3→L	49%	H-1→L+1	45%							2.62	0.0001
S10(3^1B_2)	H-3→L+1	48%	H-1→L	40%							2.62	0.0003
S11(3^1B_1)	H-3→L+2	50%	H-1→L+3	50%							2.64	0.0000
S12(3^1A_2)	H-3→L+3	51%	H-1→L+2	48%							2.64	0.0000
S13(4^1B_1)	H-4→L	87%									2.79	0.0036
S14(4^1A_2)	H-4→L+1	86%									2.80	0.0000
S15(4^1B_2)	H-4→L+3	83%									2.86	0.0169
S16(4^1A_1)	H-4→L+2	91%									2.87	0.0237
S17(5^1A_2)	H-1→L+4	99%									2.92	0.0000
S18(5^1A_1)	H→L+4	98%									2.92	0.0325
S19(5^1B_1)	H-3→L+4	99%									2.93	0.0000
S20(5^1B_2)	H-2→L+4	99%									2.95	0.0009
S21(6^1A_1)	H-4→L+4	95%									3.25	0.2699
S22(6^1B_2)	H-2→L+2	23%	H-3→L+1	22%	H-1→L	21%	H-4→L+3	15%	H→L+3	15%	3.30	0.0668
S23(6^1A_2)	H-6→L+1	48%	H-5→L	51%							3.32	0.0000
S24(6^1B_1)	H-5→L+1	48%	H-6→L	51%							3.32	0.0000
S25(7^1A_1)	H-5→L+3	49%	H-6→L+2	51%							3.33	0.0000
S26(7^1B_2)	H-5→L+2	51%	H-6→L+3	48%							3.33	0.0006
S27(7^1A_2)	H-4→L+1	11%	H-3→L+3	25%	H-2→L	22%	H→L+1	16%	H-1→L+2	23%	3.38	0.0000
S28(7^1B_1)	H-2→L+1	21%	H-3→L+2	20%	H-1→L+3	20%	H→L	14%			3.59	1.1884
S29(8^1A_1)	H-2→L+3	23%	H-3→L	20%	H-1→L+1	20%	H→L+2	17%			3.61	1.6240

$(ZnP)_2DPB$												
$S1(1^1B_2)$	H-1→L+1	46%	H→L	48%							2.31	0.0000
$S2(1^1A_2)$	H-1→L	47%	H→L+1	47%							2.31	0.0000
$S3(1^1B_1)$	H-1→L+2	27%	H→L+3	26%	H-3→L+1	24%	H-2→L	23%			2.42	0.0030
$S4(1^1A_1)$	H→L+2	28%	H-1→L+3	24%	H-2→L+1	24%	H-3→L	22%			2.42	0.0005
$S5(2^1A_2)$	H-3→L+3	14%	H-2→L+2	14%	H-1→L	37%	H→L+1	35%			2.54	0.0000
$S6(2^1B_2)$	H-1→L+1	37%	H→L	37%	H-3→L+2	16%	H-2→L+3	10%			2.54	0.0120
$S7(2^1A_1)$	H-3→L	52%	H→L+2	47%							2.56	0.0000
$S8(2^1B_1)$	H-1→L+2	23%	H→L+3	24%	H-3→L+1	29%	H-2→L	25%			2.57	0.0000
$S9(3^1B_1)$	H-1→L+2	26%	H→L+3	24%	H-3→L+1	23%	H-2→L	27%			2.58	0.0000
$S10(3^1A_1)$	H-2→L+1	50%	H-1→L+3	50%							2.58	0.0001
$S11(3^1A_2)$	H-3→L+3	47%	H-2→L+2	48%							2.68	0.0000
$S12(3^1B_2)$	H-2→L+3	48%	H-3→L+2	46%							2.68	0.0005
$S13(4^1A_2)$	H-4→L	97%									2.90	0.0000
$S14(4^1B_2)$	H-4→L+1	94%									2.93	0.0018
$S15(4^1B_1)$	H-4→L+2	97%									3.06	0.0054
$S16(4^1A_1)$	H-4→L+3	98%									3.13	0.0195
$S17(5^1B_2)$	H-1→L+4	57%	H-3→L+2	12%	H-2→L+3	15%					3.19	0.0264
$S18(5^1A_2)$	H→L+4	81%									3.20	0.0000
$S19(6^1A_2)$	H-6→L+2	30%	H-5→L	69%							3.30	0.0000
$S20(5^1B_1)$	H-6→L	69%	H-5→L+2	31%							3.31	0.0001
$S21(6^1B_2)$	H-5→L+1	66%	H-6→L+3	28%							3.31	0.0018
$S22(5^1A_1)$	H-6→L+1	69%	H-5→L+3	30%							3.31	0.0001
$S23(7^1B_2)$	H-1→L+4	32%	H-2→L+3	20%	H-3→L+2	19%					3.32	0.0383
$S24(7^1A_2)$	H-3→L+3	27%	H-2→L+2	27%	H-1→L	11%	H→L+4	18%	H→L+1	11%	3.37	0.0000
$S25(6^1B_1)$	H-3→L+4	88%									3.37	0.0814
$S26(6^1A_1)$	H-2→L+4	89%									3.41	0.1947
$S27(8^1B_2)$	H-4→L+4	89%									3.44	0.0000
$S28(8^1A_2)$	H-7→L	55%	H-8→L+1	29%							3.62	0.0000
$S29(7^1A_1)$	H-1→L+3	19%	H-2→L+1	19%	H-3→L	18%	H-2→L+4	10%	H→L+2	17%	3.64	1.4316
$S30(9^1B_2)$	H-7→L+1	59%	H-8→L	31%							3.64	0.0018
$S31(7^1B_1)$	H-3→L+1	14%	H-2→L	17%	H-1→L+2	16%	H→L+3	15%			3.65	0.9373
$(ZnP)_2DPO$												
$S1(1^1B_2)$	H→L+3	23%	H-2→L+1	25%	H-1→L	26%	H→L+2	26%			2.42	0.0000
$S2(1^1A_2)$	H-3→L+1	24%	H-1→L+2	25%	H-2→L+3	23%	H→L	27%			2.42	0.0000
$S3(1^1B_1)$	H→L+1	26%	H-2→L+2	25%	H-3→L	25%	H-1→L+3	24%			2.43	0.0047
$S4(1^1A_1)$	H-2→L	26%	H-1→L+1	25%	H→L+3	25%	H-3→L+2	24%			2.43	0.0003
$S5(2^1A_1)$	H-2→L	50%	H-1→L+1	50%							2.70	0.0000
$S6(2^1B_2)$	H-2→L+1	50%	H-1→L	50%							2.70	0.0000

$S7(2^1B_1)$	H-3→L	50%	H→L+1	50%							2.70	0.0000
$S8(2^1A_2)$	H-3→L+1	51%	H→L	49%							2.70	0.0000
$S9(3^1B_1)$	H-2→L+2	50%	H-1→L+3	50%							2.72	0.0000
$S10(3^1A_2)$	H-2→L+3	50%	H-1→L+2	50%							2.72	0.0000
$S11(3^1A_1)$	H-3→L+2	50%	H→L+3	50%							2.72	0.0000
$S12(3^1B_2)$	H-3→L+3	50%	H→L+2	50%							2.72	0.0004
$S13(4^1A_2)$	H-7→L+1	49%	H-6→L	50%							3.31	0.0000
$S14(4^1B_1)$	H-7→L	50%	H-6→L+1	49%							3.31	0.0000
$S15(4^1B_2)$	H-6→L+2	50%	H-7→L+3	49%							3.34	0.0038
$S16(4^1A_1)$	H-7→L+2	50%	H-6→L+3	49%							3.34	0.0001
$S17(5^1B_2)$	H-3→L+3	26%	H→L+2	23%	H-2→L+1	22%	H-1→L	22%			3.36	0.3378
$S18(5^1A_2)$	H-4→L	10%	H-3→L+1	22%	H-2→L+3	22%	H-1→L+2	21%	H→L	20%	3.42	0.0000
$S19(5^1B_1)$	H-4→L+1	42%	H-3→L	14%	H-2→L+2	12%	H→L+1	13%	H-1→L+3	12%	3.50	0.6862
$S20(5^1A_1)$	H-3→L+2	23%	H→L+3	23%	H-1→L+1	21%	H-2→L	21%			3.55	1.7771
$S21(6^1A_2)$	H-4→L	84%									3.58	0.0000
$S22(6^1B_1)$	H-5→L	89%									3.60	0.0800
$S23(7^1A_2)$	H-5→L+1	93%									3.60	0.0000
$S24(7^1B_1)$	H-4→L+1	49%	H-2→L+4	18%							3.61	0.4027
$S25(6^1B_2)$	H-4→L+2	93%									3.64	0.0000
$S26(6^1A_1)$	H-4→L+3	89%									3.64	0.0419
$(ZnP)_2DPS$												
$S1(1^1B_2)$	H-2→L	27%	H→L+2	24%	H-3→L+1	24%	H-1→L+3	24%			2.42	0.0001
$S2(1^1A_1)$	H-2→L+1	26%	H-3→L	25%	H→L+3	25%	H-1→L+2	24%			2.42	0.0004
$S3(1^1A_2)$	H-3→L+3	23%	H-1→L+1	25%	H-2→L+2	25%	H→L	27%			2.42	0.0000
$S4(1^1B_1)$	H-1→L	26%	H→L+1	26%	H-2→L+3	25%	H-3→L+2	23%			2.42	0.0063
$S21(6^1B_2)$	H→L+2	21%	H-1→L+3	20%	H-3→L+1	20%	H-4→L+2	15%	H-2→L	18%	3.39	0.5308
$S22(6^1A_2)$	H-5→L+1	19%	H-3→L+3	19%	H-2→L+2	18%	H→L	18%	H-1→L+1	17%	3.44	0.0000
$S23(6^1B_1)$	H-5→L	50%	H-3→L+2	11%	H-2→L+3	10%	H→L+1	11%	H-1→L	10%	3.48	0.5857
$S24(6^1A_1)$	H→L+3	23%	H-1→L+2	22%	H-3→L	21%	H-2→L+1	21%			3.54	1.6849
$(ZnP)_2DPX$												
$S3(1^1B_1)$	H→L+3	28%	H-1→L+2	27%	H-2→L	23%	H-3→L+1	22%			2.42	0.0033
$S4(1^1A_1)$	H→L+2	31%	H-1→L+3	25%	H-2→L+1	23%	H-3→L	21%			2.43	0.0001
$S5(2^1B_2)$	H-3→L+2	22%	H-2→L+3	11%	H-1→L+1	35%	H→L	32%			2.56	0.0000
$S6(2^1A_2)$	H-3→L+3	15%	H-1→L	34%	H-2→L+2	18%	H→L+1	33%			2.56	0.0000
$S15(4^1B_2)$	H-2→L+3	34%	H-3→L+2	31%	H-1→L+1	16%	H→L	15%			3.28	0.0082
$S21(6^1A_2)$	H-2→L+2	30%	H-3→L+3	32%	H→L+1	15%	H-1→L	15%			3.33	0.0000
$S23(6^1B_1)$	H-2→L	21%	H-1→L+2	21%	H-3→L+1	20%	H→L+3	19%			3.62	1.0817
$S24(6^1A_1)$	H-2→L+1	23%	H-1→L+3	23%	H-3→L	21%	H→L+2	20%			3.62	1.7342
ZnTriPP												

S1(1^1A_1)	H-1→L	48%	H→L+1	52%							2.38	0.0000
S2(1^1B_2)	H→L	53%	H-1→L+1	47%							2.38	0.0009
S3(1^1B_1)	H-2→L	100%									3.30	0.0000
S4(1^1A_2)	H-2→L+1	100%									3.30	0.0000
S5(2^1B_2)	H→L	45%	H-1→L+1	52%							3.39	1.3841
S6(2^1A_1)	H-1→L	51%	H→L+1	45%							3.40	1.0192
(ZnTriPP)$_2$DPA												
S1(1^1B_2)	H-3→L+3	19%	H-1→L+2	26%	H→L+1	27%	H-2→L	26%			2.33	0.0000
S2(1^1A_1)	H-2→L+3	27%	H-1→L+1	26%	H→L+2	26%	H-3→L	20%			2.33	0.0019
S3(1^1A_2)	H-2→L+2	27%	H-3→L+1	19%	H-1→L	27%	H→L+3	26%			2.33	0.0000
S4(1^1B_1)	H-2→L+1	28%	H→L	26%	H-1→L+3	25%	H-3→L+2	19%			2.33	0.0080
S5(2^1B_2)	H-1→L+2	50%	H→L+1	50%							2.53	0.0000
S6(2^1A_1)	H-1→L+1	50%	H→L+2	50%							2.53	0.0000
S7(2^1B_1)	H-1→L+3	50%	H→L	50%							2.53	0.0000
S8(2^1A_2)	H-1→L	49%	H→L+3	51%							2.53	0.0000
S9(3^1B_1)	H-2→L+1	54%	H-3→L+2	40%							2.57	0.0058
S10(3^1A_2)	H-3→L+1	39%	H-2→L+2	56%							2.57	0.0000
S11(3^1B_2)	H-2→L	56%	H-2→L+3	41%							2.59	0.0065
S12(3^1A_1)	H-2→L+3	53%	H-3→L	46%							2.59	0.0063
S13(4^1B_1)	H-4→L+1	81%	H-3→L+2	15%							2.78	0.0222
S14(4^1A_2)	H-4→L+2	77%	H-3→L+1	17%							2.78	0.0000
S15(4^1B_2)	H-4→L	76%	H-3→L+3	15%							2.81	0.0307
S16(5^1A_2)	H→L+4	99%									2.84	0.0000
S17(4^1A_1)	H-4→L+3	88%									2.84	0.0528
S18(5^1B_1)	H-1→L+4	99%									2.84	0.0001
S19(5^1A_1)	H-2→L+4	98%									2.91	0.0536
S20(5^1B_2)	H-3→L+4	99%									2.95	0.0003
S21(6^1B_2)	H-3→L+3	25%	H-4→L	20%	H-1→L+2	19%	H-2→L	14%	H→L+1	19%	3.18	0.1455
S22(6^1A_2)	H-3→L+1	25%	H-4→L+2	17%	H-2→L+2	16%	H-1→L	20%	H→L+3	20%	3.20	0.0000
S23(6^1A_1)	H-4→L+4	90%									3.25	0.5015
S24(7^1A_2)	H-6→L+2	49%	H-5→L+1	50%							3.28	0.0000
S25(6^1B_1)	H-6→L+1	50%	H-5→L+2	49%							3.28	0.0006
S26(7^1B_2)	H-6→L	50%	H-5→L+3	49%							3.29	0.0001
S27(7^1A_1)	H-6→L+3	49%	H-5→L	50%							3.29	0.0000
S28(7^1B_1)	H-3→L+2	25%	H-1→L+3	20%	H→L	20%	H-4→L+1	13%	H-2→L+1	16%	3.41	2.3128
S29(8^1A_1)	H-3→L	23%	H→L+2	19%	H-1→L+1	19%	H-2→L+3	16%			3.42	1.5154
(ZnTriPP)$_2$DPB												
S1(1^1B_2)	H-1→L+3	10%	H→L+1	47%	H-3→L+2	10%	H-2→L	32%			2.30	0.0004
S2(1^1A_2)	H-3→L+3	10%	H-2→L+1	30%	H→L	51%					2.30	0.0000
S3(1^1A_1)	H-1→L+1	30%	H→L+3	24%	H-3→L	23%	H-2→L+2	23%			2.33	0.0028
S4(1^1B_1)	H-1→L	31%	H→L+2	25%	H-3→L+1	22%	H-2→L+3	21%			2.33	0.0158
S5(2^1B_1)	H-1→L	48%	H→L+2	52%							2.48	0.0000
S6(2^1A_2)	H-1→L+2	59%	H→L	32%							2.49	0.0000
S7(2^1A_1)	H→L+3	53%	H-1→L+1	47%							2.49	0.0001
S8(2^1B_2)	H-1→L+3	55%	H→L+1	36%							2.50	0.0069
S9(3^1A_1)	H-3→L	50%	H-2→L+2	50%							2.59	0.0002
S10(3^1B_2)	H-3→L+2	51%	H-2→L	40%							2.59	0.0089
S11(3^1B_1)	H-3→L+1	49%	H-2→L+3	51%							2.60	0.0000
S12(3^1A_2)	H-3→L+3	51%	H-2→L+1	42%							2.60	0.0000
S13(4^1A_2)	H-4→L+1	94%									2.90	0.0000

S14(4^1B_2)	H-4→L	90%									2.91	0.0081
S15(4^1B_1)	H-4→L+3	96%									2.99	0.0195
S16(4^1A_1)	H-4→L+2	98%									3.02	0.0275
S17(5^1B_2)	H-3→L+2	31%	H-1→L+3	22%	H-2→L	15%	H-2→L+4	10%	H→L+1	13%	3.12	0.1809
S18(5^1A_2)	H-3→L+3	24%	H-1→L+2	18%	H-2→L+1	13%	H→L+4	30%	H→L	11%	3.13	0.0000
S19(5^1B_1)	H-1→L+4	80%									3.24	0.2711
S20(6^1A_2)	H-3→L+3	10%	H→L+4	69%							3.25	0.0000
S21(6^1B_2)	H-6→L+2	41%	H-5→L	58%							3.28	0.0000
S22(5^1A_1)	H-6→L	58%	H-5→L+2	41%							3.28	0.0022
S23(7^1A_2)	H-6→L+3	40%	H-5→L+1	59%							3.28	0.0000
S24(6^1B_1)	H-6→L+1	58%	H-5→L+3	40%							3.28	0.0001
S25(7^1B_2)	H-4→L+4	16%	H-2→L+4	72%							3.32	0.0193
S26(6^1A_1)	H-3→L	14%	H-3→L+4	45%	H-2→L+2	15%	H-1→L+1	11%	H→L+3	12%	3.35	1.0558
S27(7^1B_1)	H-3→L+1	21%	H-2→L+3	20%	H-1→L	15%	H→L+2	16%	H-1→L+4	18%	3.44	2.0516
S29(7^1A_1)	H-3→L	10%	H-3→L+4	54%	H-2→L+2	11%	H→L+3	10%			3.47	0.8018
$(ZnTriPP)_2DPO$												
S1(1^1B_2)	H→L	28%	H-1→L+2	27%	H-2→L+1	23%	H-3→L+3	21%			2.34	0.0008
S2(1^1A_1)	H-1→L	27%	H→L+2	27%	H-2→L+3	23%	H-3→L+1	22%			2.34	0.0039
S3(1^1A_2)	H-1→L+3	26%	H-3→L+2	21%	H-2→L	23%	H→L+1	28%			2.34	0.0000
S4(1^1B_1)	H-1→L+1	28%	H→L+3	26%	H-2→L+2	22%	H-3→L	22%			2.34	0.0092
S5(2^1A_1)	H-1→L	50%	H→L+2	50%							2.58	0.0000
S6(2^1B_2)	H-1→L+2	50%	H→L	50%							2.58	0.0000
S7(2^1B_1)	H-1→L+1	50%	H→L+3	50%							2.58	0.0000
S8(2^1A_2)	H-1→L+3	51%	H→L+1	49%							2.58	0.0000
S9(3^1A_2)	H-3→L+2	50%	H-2→L	50%							2.67	0.0000
S10(3^1B_1)	H-3→L	50%	H-2→L+2	50%							2.67	0.0000
S11(3^1B_2)	H-3→L+3	50%	H-2→L+1	50%							2.68	0.0005
S12(3^1A_1)	H-3→L+1	50%	H-2→L+3	50%							2.68	0.0000
S13(4^1B_2)	H-3→L+3	29%	H-2→L+1	26%	H-1→L+2	21%	H→L	21%			3.20	0.3317
S14(4^1A_2)	H-3→L+2	28%	H-2→L	26%	H-1→L+3	22%	H→L+1	21%			3.22	0.0000
S15(5^1A_2)	H-7→L+2	49%	H-6→L	50%							3.28	0.0000
S16(4^1B_1)	H-7→L	50%	H-6→L+2	49%							3.28	0.0000
S17(4^1A_1)	H-7→L+1	50%	H-6→L+3	49%							3.29	0.0012
S18(5^1B_2)	H-6→L+1	50%	H-7→L+3	49%							3.29	0.0004
S19(5^1B_1)	H-3→L	25%	H-2→L+2	23%	H→L+3	20%	H-1→L+1	19%			3.36	2.1082
S20(5^1A_1)	H-3→L+1	26%	H-2→L+3	26%	H→L+2	21%	H-1→L	21%			3.39	1.9706
$(ZnTriPP)_2DPS$												
S1(1^1B_2)	H→L	30%	H-1→L+1	26%	H-2→L+2	22%	H-3→L+3	21%			2.33	0.0024
S2(1^1A_1)	H→L+1	27%	H-1→L	27%	H-2→L+3	23%	H-3→L+2	22%			2.34	0.0038
S3(1^1A_2)	H→L+2	28%	H-1→L+3	26%	H-2→L	24%	H-3→L+1	22%			2.34	0.0000
S4(1^1B_1)	H→L+3	28%	H-1→L+2	26%	H-3→L	23%	H-2→L+1	23%			2.34	0.0087
S15(4^1B_2)	H-4→L+2	34%	H-3→L+3	20%	H-2→L+2	17%	H→L	13%	H-1→L+1	14%	3.17	0.4959
S17(5^1A_2)	H-4→L	19%	H-3→L+1	20%	H-2→L	21%	H→L+2	17%	H-1→L+3	18%	3.27	0.0000
S23(6^1B_1)	H-2→L+1	22%	H-3→L	21%	H-1→L+2	18%	H-4→L+1	10%	H→L+3	18%	3.35	2.0584
S24(6^1A_1)	H-2→L+3	25%	H-3→L+2	25%	H-1→L	20%	H→L+1	20%			3.37	1.7907
$(ZnTriPP)_2DPX$												
S1(1^1B_2)	H→L+1	35%	H-2→L	25%	H-1→L+3	21%	H-3→L+2	19%			2.33	0.0001
S2(1^1A_2)	H-3→L+3	18%	H-1→L+2	22%	H-2→L+1	25%	H→L	34%			2.33	0.0000
S3(1^1A_1)	H-1→L+1	27%	H→L+3	27%	H-2→L+2	23%	H-3→L	22%			2.33	0.0040
S4(1^1B_1)	H→L+2	29%	H-1→L	26%	H-3→L+1	22%	H-2→L+3	22%			2.33	0.0143

S13(4^1B_2)	H-3→L+2	28%	H-2→L	26%	H-1→L+3	23%	H→L+1	20%			3.16	0.1038
S14(4^1A_2)	H-3→L+3	29%	H-2→L+1	25%	H-1→L+2	21%	H→L	19%			3.16	0.0000
S23(6^1B_1)	H-2→L+3	26%	H-3→L+1	26%	H-1→L	21%	H→L+2	20%			3.39	2.3041
S24(6^1A_1)	H-3→L	26%	H-2→L+2	26%	H→L+3	21%	H-1→L+1	21%			3.40	1.9957

Table 5: Effects of solvation by benzene and the use of a diffuse function and a functional including dispersion on the optimized geometry, MO energies and vertical excitation energies of $(ZnP)_2$DPB and $(ZnP)_2$DPS.

$(ZnP)_2$DPB	**1**	**2**	**3**	**4**	**5**
D_1 (A-B) Distance (Å)	3.842	3.847	3.864	3.791	3.797
D_2 (C-D) Distance (Å)	3.970	4.003	4.056	3.755	3.772
D_3 (Zn(1)-Zn(2)) Distance (Å)	4.433	4.694	4.764	3.622	3.649
D_4 (Zn-N_4) Av. Displacement (Å)	0.011	0.019	0.015	0.014	0.019
D_5 (P_1-P_2) Distance (Å)	4.456	4.732	4.794	3.650	3.687
D_6 Mean Plane Separation (Å)	4.466	4.730	4.801	3.663	3.726
β InterplanarAngle (°)	7.77	12.56	11.67	0.72	0.41
α Slip Angle (°)	3.83	6.22	5.83	1.34	0
D_7 Lateral Shift (Å)	0.30	0.51	0.49	0.08	0
HOMO (eV)	-4.97	-5.04	-5.30	-4.75	-5.09
LUMO (eV)	-2.09	-2.14	-2.44	-2.24	-2.61
Q band (eV)	2.42	2.41	2.38	2.42	2.38
Soret band (eV)	3.64	3.37	3.57	3.68	3.37
$(ZnP)_2$DPS	**1**	**2**	**3**	**4**	**5**
D_1 (A-B) Distance (Å)	5.281	5.282	5.282	5.265	5.267
D_2 (C-D) Distance (Å)	6.392	6.374	6.378	6.310	6.295
D_3 (Zn(1)-Zn(2)) Distance (Å)	8.958	8.774	8.871	8.571	8.485
D_4 (Zn-N_4) Av. Displacement (Å)	0.015	0.018	0.004	0.013	0.003
D_5 (P_1-P_2) Distance (Å)	8.984	8.807	8.878	8.597	8.490
D_6 Mean Plane Separation (Å)	8.344	8.267	8.292	8.097	8.035
β InterplanarAngle (°)	43.58	40.26	41.82	38.81	37.13
α Slip Angle (°)	21.79	20.11	20.92	19.41	18.56
D_7 Lateral Shift (Å)	3.33	3.03	3.17	2.86	2.70
HOMO (eV)	-5.15	-5.20	-5.45	-5.15	-5.46
LUMO (eV)	-2.13	-2.19	-2.47	-2.13	-2.49
Q band (eV)	2.42	2.41	2.38	2.42	2.37
Soret band (eV)	3.54	3.34	3.46	3.54	3.26

1. B3LYP/6-31G(d)*in vacuo*.
2. B3LYP/6-31G(d) in benzene solvent.
3. B3LYP/6-31+G(d,p) *in vacuo*.
4. B3LYP-D3/6-31G(d) *in vacuo*
5. B3LYP-D3/6-31+G(d,p) in benzene solvent.

Table 6: Excitation energies (in eV) of electron spin forbidden transitions to triplet excited states inthe dimers $(ZnP)_2X$ and $(ZnTriPP)_2X$, where (X = DPA, DPB, DPO, DPS, DPX), obtained at the TD-B3LYP/6-31G(d) level of theory *in vacuo* with a C_{2v} symmetry constraint.

States	Composition of Transitions										E(eV)
ZnP											
T_1 (1^3E_u)	H-1→L	71%	H→L+1	28%							1.77
T_2 (2^3E_u)	H-1→L	28%	H→L+1	72%							2.08
$(ZnP)_2$DPA											
T_1 (1^3A_1)	H-3→L	36%	H-1→L+1	36%	H-2→L+3	12%	H→L+2	10%	H-4→L+2	2%	1.75
T_2 (1^3B_2)	H-3→L+1	36%	H-2→L+2	13%	H-1→L	38%	H→L+3	11%			1.75
T_3 (1^3A_2)	H-3→L+3	33%	H-1→L+2	35%	H-2→L	16%	H→L+1	14%			1.76
T_4 (1^3B_1)	H-3→L+2	34%	H-1→L+3	34%	H-2→L+1	15%	H→L	14%			1.76
T_5 (2^3A_1)	H-4→L+4	63%	H-15→L+8	3%	H→L+4	31%					1.78
T_6 (2^3B_1)	H-3→L+2	16%	H-2→L+1	33%	H-1→L+3	16%	H-4→L	4%	H→L	32%	2.05
T_7 (2^3A_2)	H-3→L+3	15%	H-2→L	34%	H-1→L+2	16%	H-4→L+1	3%	H→L	31%	2.05
T_8 (2^3B_2)	H-3→L+1	12%	H-2→L+2	37%	H-1→L	13%	H-4→L+3	4%	H→L+3	33%	2.06
T_9 (3^3A_1)	H-3→L	13%	H-2→L+3	36%	H-1→L+1	13%	H-4→L+2	4%	H→L+2	34%	2.06
$(ZnP)_2$DPB											
T_1 (1^3B_2)	H-3→L+2	23%	H-1→L+1	16%	H→L	51%	H-2→L+3	8%			1.72
T_2 (1^3A_2)	H-3→L+3	22%	H→L+1	49%	H-1→L	19%	H-2→L+2	9%			1.73
T_3 (1^3A_1)	H-3→L	36%	H-2→L+1	12%	H-1→L+3	13%	H→L+2	38%			1.75
T_4 (1^3B_1)	H-3→L+1	34%	H-2→L	14%	H-1→L+2	15%	H→L+3	36%			1.76
T_5 (2^3A_2)	H-2→L+2	17%	H-1→L	54%	H→L+1	22%	H-3→L+3	6%			2.01
T_6 (2^3B_2)	H-2→L+3	17%	H-1→L+1	57%	H-3→L+2	6%	H→L	19%			2.01
T_7 (2^3B_1)	H-3→L+1	14%	H-2→L	35%	H-1→L+2	36%	H→L+3	15%			2.06
T_8 (2^3A_1)	H-3→L	12%	H-2→L+1	36%	H-1→L+3	38%	H→L+2	13%			2.06
$(ZnP)_2$DPO											
T_1 (1^3B_2)	H-3→L+3	12%	H-1→L	38%	H→L+2	12%	H-2→L+1	37%			1.75
T_2 (1^3A_1)	H-3→L+2	12%	H→L+3	12%	H-1→L+1	37%	H-2→L	37%			1.75
T_3 (1^3A_2)	H-3→L+1	15%	H-2→L+3	34%	H-1→L+2	34%	H→L	16%			1.77
T_4 (1^3B_1)	H-3→L	16%	H-1→L+3	34%	H→L+1	16%	H-2→L+2	34%			1.77
T_5 (2^3A_2)	H-3→L+1	34%	H-2→L+3	16%	H-1→L+2	16%	H→L	35%			2.06
T_6 (2^3B_1)	H-3→L	34%	H-2→L+2	16%	H-1→L+3	16%	H→L+1	35%			2.06
T_7 (2^3B_2)	H-3→L+3	37%	H-2→L+1	12%	H-1→L	13%	H→L+2	38%			2.07
T_8 (2^3A_1)	H-3→L+2	37%	H-2→L	12%	H-1→L+1	12%	H→L+3	38%			2.07
$(ZnP)_2$DPS											
T_1 (1^3B_2)	H-3→L+1	36%	H-1→L+3	12%	H→L+2	12%	H-2→L	38%			1.75
T_2 (1^3A_1)	H-3→L	37%	H→L+3	12%	H-1→L+2	12%	H-2→L+1	37%			1.75
T_3 (1^3A_2)	H-3→L+3	32%	H-2→L+2	33%	H-1→L+1	17%	H→L	17%			1.77
T_4 (1^3B_1)	H-3→L+2	32%	H-2→L+3	33%	H-1→L	17%	H→L+1	17%			1.77
T_5 (2^3A_2)	H-3→L+3	17%	H-2→L+2	18%	H-1→L+1	32%	H→L	33%			2.05
T_6 (2^3B_1)	H-3→L+2	17%	H-2→L+3	18%	H-1→L	33%	H→L+1	32%			2.05
T_7 (2^3A_1)	H-3→L	12%	H-2→L+1	13%	H-1→L+2	37%	H→L+3	37%			2.07
T_8 (2^3B_2)	H-3→L+1	12%	H-2→L	13%	H-1→L+3	37%	H→L+2	38%			2.07
$(ZnP)_2$DPX											
T_1 (1^3B_2)	H-3→L+2	26%	H-1→L+1	16%	H-2→L+3	9%	H→L	49%			1.73
T_2 (1^3A_2)	H-3→L+3	24%	H-2→L+2	10%	H-1→L	19%	H→L+1	47%			1.74

T_3 (1^3A_1)	H-3→L	36%	H-2→L+1	12%	H-1→L+3	13%	H→L+2	39%			1.75
T_4 (1^3B_1)	H-3→L+1	34%	H-2→L	14%	H-1→L+2	15%	H→L+3	36%			1.76
T_5 (2^3A_2)	H-2→L+2	20%	H-1→L	51%	H→L+1	21%	H-3→L+3	8%			2.03
T_6 (2^3B_2)	H-2→L+3	21%	H-3→L+2	7%	H-1→L+1	54%	H→L	18%			2.03
T_7 (2^3B_1)	H-3→L+1	14%	H-2→L	34%	H-1→L+2	37%	H→L+3	16%			2.06
T_8 (2^3A_1)	H-3→L	12%	H-2→L+1	37%	H-1→L+3	38%	H→L+2	13%			2.06
ZnTriP											
T_1 (1^3B_2)	H-1→L+1	21%	H→L	78%							1.72
T_2 (1^3A_1)	H-1→L	22%	H→L+1	77%							1.72
T_3 (2^3A_1)	H-1→L	78%	H→L+1	22%							2.04
T_4 (2^3B_2)	H-1→L+1	78%	H→L	22%							2.04
$(ZnTriPP)_2DPA$											
T_1 (1^3A_1)	H-3→L	9%	H-1→L+1	40%	H-2→L+3	8%	H→L+2	40%			1.68
T_2 (1^3B_2)	H-1→L+2	40%	H-3→L+3	9%	H-2→L	8%	H→L+1	41%			1.68
T_3 (1^3B_1)	H-3→L+2	10%	H-1→L+3	38%	H-2→L+1	10%	H→L	39%			1.70
T_4 (1^3A_2)	H-3→L+1	10%	H-1→L	39%	H-2→L+2	10%	H→L+3	39%			1.70
T_5 (2^3A_1)	H-4→L+4	62%	H-2→L+4	35%	H-28→L+20	3%					1.77
T_6 (2^3B_1)	H-3→L+2	37%	H-2→L+1	37%	H-1→L+3	11%	H-4→L+1	4%	H→L	11%	2.01
T_7 (2^3A_2)	H-3→L+1	37%	H-2→L+2	37%	H-1→L	11%	H-4→L+2	4%	H→L+3	11%	2.01
T_8 (2^3B_2)	H-3→L+3	38%	H-2→L	38%	H-1→L+2	9%	H-4→L	5%	H→L+1	9%	2.01
$(ZnTriPP)_2DPB$											
T_1 (1^3B_2)	H→L+1	48%	H-3→L+2	8%	H-2→L	10%	H-1→L+3	33%			1.67
T_2 (1^3A_2)	H→L	47%	H-2→L+1	11%	H-1→L+2	34%	H-3→L+3	8%			1.68
T_3 (1^3A_1)	H-3→L	9%	H-2→L+2	9%	H-1→L+1	41%	H→L+3	40%			1.68
T_4 (1^3B_1)	H-3→L+1	9%	H-2→L+3	9%	H-1→L	40%	H→L+2	40%			1.68
T_5 (2^3B_2)	H-3→L+2	31%	H-2→L	50%	H→L+1	12%	H-1→L+3	7%			2.01
T_6 (2^3A_2)	H-3→L+3	30%	H-2→L+1	51%	H-1→L+2	7%	H→L	12%			2.01
T_7 (2^3A_1)	H-3→L	40%	H-2→L+2	41%	H-1→L+1	9%	H→L+3	9%			2.02
T_8 (2^3B_1)	H-3→L+1	41%	H-2→L+3	40%	H-1→L	9%	H→L+2	9%			2.02
$(ZnTriPP)_2DPO$											
T_1 (1^3B_2)	H-3→L+3	9%	H-1→L+2	40%	H→L	41%	H-2→L+1	9%			1.69
T_2 (1^3A_1)	H-3→L+1	9%	H→L+2	41%	H-1→L	41%	H-2→L+3	9%			1.69
T_3 (1^3A_2)	H-3→L+2	10%	H-2→L	11%	H-1→L+3	39%	H→L+1	39%			1.70
T_4 (1^3B_1)	H-3→L	10%	H-1→L+1	39%	H→L+3	39%	H-2→L+2	11%			1.70
T_5 (2^3A_2)	H-3→L+2	38%	H-2→L	40%	H-1→L+3	11%	H→L+1	11%			2.02
T_6 (2^3B_1)	H-3→L	39%	H-2→L+2	40%	H-1→L+1	11%	H→L+3	11%			2.02
T_7 (2^3B_2)	H-3→L+3	40%	H-2→L+1	42%	H-1→L+2	9%	H→L	9%			2.03
T_8 (2^3A_1)	H-3→L+1	41%	H-2→L+3	41%	H-1→L	9%	H→L+2	9%			2.03
$(ZnTriPP)_2DPS$											
T_1 (1^3B_2)	H-1→L+1	40%	H-3→L+3	9%	H→L	42%	H-2→L+2	9%			1.69
T_2 (1^3A_1)	H-1→L	40%	H→L+1	41%	H-3→L+2	9%	H-2→L+3	9%			1.69
T_3 (1^3A_2)	H-3→L+1	11%	H-2→L	12%	H-1→L+3	37%	H→L+2	39%			1.70
T_4 (1^3B_1)	H-3→L	12%	H-2→L+1	11%	H-1→L+2	38%	H→L+3	38%			1.70
T_5 (2^3A_2)	H-3→L+1	38%	H-2→L	39%	H-1→L+3	11%	H→L+2	12%			2.01
T_6 (2^3B_1)	H-3→L	38%	H-2→L+1	38%	H-1→L+2	11%	H→L+3	12%			2.01
T_7 (2^3A_1)	H-3→L+2	41%	H-2→L+3	41%	H-1→L	9%	H→L+1	9%			2.02
T_8 (2^3B_2)	H-3→L+3	40%	H-2→L+2	41%	H-1→L+1	9%	H→L	9%			2.02
$(ZnTriPP)_2DPX$											
T_1 (1^3B_2)	H-3→L+2	9%	H-1→L+3	38%	H-2→L	9%	H→L+1	43%			1.68
T_2 (1^3A_1)	H-1→L+1	41%	H-2→L+2	9%	H-3→L	9%	H→L+3	41%			1.68

T_3 (1^3A_2)	H-3→L+3	9%	H-2→L+1	10%	H-1→L+2	38%	H→L	42%			1.68
T_4 (1^3B_1)	H-3→L+1	10%	H-2→L+3	10%	H-1→L	40%	H→L+2	40%			1.68
T_5 (2^3B_2)	H-2→L	43%	H→L+1	10%	H-1→L+3	8%	H-3→L+2	38%			2.02
T_6 (2^3A_2)	H-2→L+1	43%	H-3→L+3	37%	H-1→L+2	9%	H→L	10%			2.02
T_7 (2^3A_1)	H-3→L	40%	H-2→L+2	41%	H-1→L+1	9%	H→L+3	9%			2.02
T_8 (2^3B_1)	H-3→L+1	40%	H-2→L+3	40%	H-1→L	10%	H→L+2	10%			2.02